

Revealing nonergodic dynamics in living cells from a single particle trajectory

Yann Lanoiselée and Denis S. Grebenkov*

Laboratoire de Physique de la Matière Condensée (UMR 7643), CNRS—Ecole Polytechnique, 91128 Palaiseau, France

(Received 18 December 2015; published 26 May 2016)

We propose the improved ergodicity and mixing estimators to identify nonergodic dynamics from a single particle trajectory. The estimators are based on the time-averaged characteristic function of the increments and can thus capture additional information on the process as compared to the conventional time-averaged mean-square displacement. The estimators are first investigated and validated for several models of anomalous diffusion, such as ergodic fractional Brownian motion and diffusion on percolating clusters, and nonergodic continuous-time random walks and scaled Brownian motion. The estimators are then applied to two sets of earlier published trajectories of mRNA molecules inside live *Escherichia coli* cells and of Kv2.1 potassium channels in the plasma membrane. These statistical tests did not reveal nonergodic features in the former set, while some trajectories of the latter set could be classified as nonergodic. Time averages along such trajectories are thus not representative and may be strongly misleading. Since the estimators do not rely on ensemble averages, the nonergodic features can be revealed separately for each trajectory, providing a more flexible and reliable analysis of single-particle tracking experiments in microbiology.

DOI: [10.1103/PhysRevE.93.052146](https://doi.org/10.1103/PhysRevE.93.052146)

I. INTRODUCTION

Statistical analysis of a single random realization of an unknown stochastic process has become indispensable in various fields, from geosciences to microbiology and finances. In these fields, multiple realizations of a process are either impossible due to the nonrepeatable unique character of observations (e.g., earth vibrations or stock prices), or undesirable due to spatial heterogeneity or time evolution of the medium (e.g., motion inside living cells). One therefore needs to resort to single observations to construct a mathematical or physical model of the unknown process, while the model calibration has to rely on the (implicit) ergodicity assumption to interchange ensemble and time averages. However, the ergodicity can fail in active or aging systems such as living cells [1–3], viscoelastic media [4], or blinking nanocrystals [5–7]. A finite length of acquired trajectories and randomness of estimators make challenging verifications of ergodicity in single-particle tracking (SPT) experimental data. At the same time, this is a necessary step toward reliable biophysical interpretations: if the ergodicity breaking remains undetected, any conclusion based on time averages along a single trajectory may be strongly misleading.

The ergodicity breaking has been thoroughly investigated for various processes, including anomalous diffusions (see Refs. [8–10] and references therein). In particular, the Khinchin's theorem relates ergodicity to the long-time vanishing of the velocity autocorrelation function (VAF) of a stationary process [11–13]. The ergodicity breaking (EB) parameter that characterizes the normalized variance of the time-averaged mean-squared displacement (TAMSD), was introduced to quantify deviations from ergodicity in numerous models of anomalous diffusion [8,9]. Since both the VAF and the EB parameter rely on ensemble averages, many trajectories are needed to reveal ergodicity breaking.

Magdziarz and Weron proposed ergodicity and mixing estimators based on a single particle trajectory [14]. For

a discrete process $Y(n)$, representing the *increments* of a trajectory $X(n)$, $Y(n) = X(n+1) - X(n)$, they introduced the functional

$$E(n) \equiv \langle \exp\{i[Y(n) - Y(0)]\} \rangle - |\langle \exp\{iY(0)\} \rangle|^2, \quad (1)$$

where $\langle \dots \rangle$ denotes the ensemble average. This functional fully characterizes the mixing and ergodic properties of stationary infinitely divisible (SID) processes: a SID process is mixing (respectively, ergodic) if and only if $E(n) \rightarrow 0$ (respectively, of $n^{-1} \sum_{k=0}^{n-1} E(k) \rightarrow 0$) as $n \rightarrow \infty$ (note that mixing implies ergodicity). The mixing and ergodicity estimators were then obtained by replacing the ensemble average in Eq. (1) by the time average along a single trajectory with $N+1$ increments $Y(0), Y(1), \dots, Y(N)$:

$$\hat{E}(n) \equiv \frac{1}{N-n+1} \sum_{k=0}^{N-n} e^{i[Y(k+n)-Y(k)]} - \left| \sum_{k=0}^N \frac{e^{iY(k)}}{N+1} \right|^2. \quad (2)$$

The smallness of $\hat{E}(n)$ (respectively, of $n^{-1} \sum_{k=0}^{n-1} \hat{E}(k)$) for large n is the necessary condition for mixing (respectively, ergodicity), whereas violation of this condition reveals the mixing (respectively, ergodicity) breaking. We emphasize that the estimators based on a single trajectory allow one to reject, with some degree of certainty, the mixing or ergodicity hypothesis but they cannot affirm it. For instance, the smallness of the estimator $\hat{E}(n)$ does not imply mixing.

Several important issues need to be resolved for reliable ergodicity assessing: (i) the smallness of the estimators needs to be quantified (e.g., by comparing the mean estimator to its standard deviation or by determining the confidence intervals, see Ref. [15]); (ii) the impact of a finite trajectory length due to which the estimators can be relatively large even for mixing and ergodic processes, should be reduced and controlled; (iii) a small bias to which the original estimators converge as n increases has to be corrected; and (iv) the failure to identify the nonergodic continuous time random walk (CTRW) as nonergodic should be amended. This last point was the major motivation for our work because macromolecular crowding

*denis.grebenkov@polytechnique.edu

strongly affects the intracellular and membrane transport [16–18] and can yield nonergodic features which are often modeled by nonstationary CTRW [2,4]. As a consequence, a reliable analysis of single-particle tracking in living cells urges for developing statistical tests to identify single trajectories for which time averages are not representative, either due to ergodicity breaking, or nonstationarity of the process.

The paper is organized as follows. In Sec. II, we present the main results: the improved estimators, their validation for anomalous diffusion models, and application to experimental data. To make this section more accessible to a broad readership, most theoretical and technical details have been moved to the discussion in Sec. III and the Appendices. In Sec. IV, we summarize the main findings and conclude.

II. RESULTS

A. Improved estimators

In this paper, we resolve the above issues by modifying the mixing estimator as

$$\hat{E}_\omega(n, N) \equiv \frac{1}{N-n+1} \sum_{k=0}^{N-n} e^{i\omega[X(k+n)-X(k)]} - \frac{1}{N(N+1)} \left| \sum_{k=0}^N e^{i\omega[X(k)-X(0)]} \right|^2 + \frac{1}{N}. \quad (3)$$

The first term can be interpreted as the time-averaged characteristic function of the increment $X(k+n) - X(k)$ at lag time n , while the second term ensures that the estimator is strictly 0 for a constant process $X(n) = X_0$ (in addition, the mean estimator is strictly 0 for a process with independent $X(n)$). The ergodicity estimator generalizes to

$$\hat{F}_\omega(n, N) \equiv \frac{1}{n} \sum_{k=1}^n \hat{E}_\omega(k, N), \quad (4)$$

where the summation over k was shifted from the original range $0, \dots, n-1$ for convenience.

There are three modifications with respect to the original estimators: (i) we consider all Fourier modes, not only $\omega = 1$, (ii) we partly remove the bias by subtracting the constant term from the second sum and changing accordingly the normalization, and (iii) most importantly, we apply the estimators to the *long-time increments* (or *positions*) of a trajectory, not to the *short-time increments* (or *velocities*); see further discussion in Sec. III A. Note that each coordinate of a two- or three-dimensional trajectory is considered separately, i.e., $X(n)$ is restricted to be a one-dimensional process. Formally, the inclusion of the frequency ω can be seen as rescaling of the process [54]. While such a rescaling does not change the mixing or ergodic property of the process and is thus redundant in the limit $n \rightarrow \infty$, high-frequency modes with large ω become important for a finite-length trajectory. Even though the changes between Eqs. (2) and (3) are minor, the application of the improved estimators to the positions of a tracer is the key feature. Rederiving the properties of the new estimators from scratch, we manage to reveal the nonergodic character of both model and experimental diffusive processes from a single trajectory.

B. Theoretical results for anomalous diffusion models

To investigate the improved mixing and ergodicity estimators (3) and (4), we consider several models of anomalous diffusion: fractional Brownian motion (fBm) [19,20], diffusion on percolating clusters [21], CTRW [22,23], and scaled Brownian motion (sBm) [24,25]. The first two processes are ergodic while the last two are not (note that the sBm exhibits the “mild nonergodicity,” for which the EB parameter vanishes with the increasing trajectory length [24,25]). We also consider CTRW with exponential cutoff, which exhibits nonergodic features at short times and becomes ergodic at longer times. Finally, we will test geometric Brownian motion (gBm), which was reported to be nonergodic [26].

The fBm at discrete time steps is a centered Gaussian process with $\langle [X(k+n) - X(k)]^2 \rangle = \sigma^2 n^{2H}$, where σ^2 is the variance of one-step displacement, and $0 < H < 1$ is the Hurst exponent. Using the identity

$$\langle e^{i\omega[X(k+n)-X(k)]} \rangle = e^{-\frac{1}{2}\omega^2 \langle [X(k+n)-X(k)]^2 \rangle}, \quad (5)$$

which is valid for any discrete centered Gaussian process, we compute

$$\langle \hat{E}_\omega(n, N) \rangle = q^{n^{2H}} - 2 \sum_{k=1}^N \frac{N+1-k}{N(N+1)} q^{k^{2H}}, \quad (6)$$

$$\langle \hat{F}_\omega(n, N) \rangle = \frac{1}{n} \sum_{k=1}^n q^{k^{2H}} - 2 \sum_{k=1}^N \frac{N+1-k}{N(N+1)} q^{k^{2H}}, \quad (7)$$

where $q = e^{-\omega^2 \sigma^2 / 2}$. For Brownian motion ($H = 1/2$), one gets explicitly

$$\langle \hat{E}_\omega(n, N) \rangle = q^n - \frac{2q(1 - \frac{1-q^{N+1}}{(N+1)(1-q)})}{N(1-q)}, \quad (8)$$

$$\langle \hat{F}_\omega(n, N) \rangle = q \frac{1-q^n}{n(1-q)} - \frac{2q(1 - \frac{1-q^{N+1}}{(N+1)(1-q)})}{N(1-q)}. \quad (9)$$

Both $\langle \hat{E}_\omega(n, N) \rangle$ and $\langle \hat{F}_\omega(n, N) \rangle$ monotonously decrease with n and approach to the limit given by the second term, but the decrease of the mean ergodicity estimator is much slower (as $1/n$). For both estimators, the second term presents the bias, which vanishes as either $N \rightarrow \infty$ or $\omega \rightarrow \infty$. While the trajectory length N is fixed by experimental setup, the frequency ω of the estimator can be increased at will. Note that the mean of the original estimator Eq. (2) contains the term $-1/(N+1)$, which could not be removed by varying ω .

For fixed n and N , the mean mixing estimator $\langle \hat{E}_\omega(n, N) \rangle$ from Eq. (8) as a function of ω exhibits nonmonotonous behavior. When $n \ll N$ and $N \gg 1$, the estimator can be approximated as $q^n - \frac{2}{N(1-q)}$ that reaches the maximum at $\sigma \omega_c \simeq (8/(nN))^{1/4}$. As a consequence, the estimator with $\omega = 1$ would classify Brownian motion with $\sigma \lesssim (8/N)^{1/4}$ as a nonergodic process. This finite-length effect can be eliminated by varying the frequency ω (see Sec. III B).

The variance of the mixing estimator,

$$\text{var}\{\hat{E}_\omega(n, N)\} = \langle |\hat{E}_\omega(n, N)|^2 \rangle - |\langle \hat{E}_\omega(n, N) \rangle|^2, \quad (10)$$

is dominated by the first term in Eq. (3), which at large $\sigma\omega$ becomes (Appendix A)

$$\text{var}\{\hat{E}_\infty(n,N)\} \simeq \frac{1}{N-n+1}. \quad (11)$$

As expected, the variance is of the order of $1/N$ for small n but progressively grows up to 1 at $n=N$. In turn, the variance of the ergodicity estimator is much smaller, as can be seen from its large ω asymptotic limit (Appendix A),

$$\text{var}\{\hat{F}_\infty(n,N)\} \simeq \frac{1}{n^2} \sum_{k=1}^n \frac{1}{N-k+1}. \quad (12)$$

When $1 \ll n \ll N$, the sum can be approximated as $\ln[N/(N-n+1)] \simeq n/N$, i.e., the variance decreases with n as $1/(nN)$, in contrast to the increasing variance of the mixing estimator in Eq. (11). In other words, summing contributions from different lag times greatly reduces fluctuations so that the ergodicity estimator applied to a single trajectory yields less noisy results.

We now turn to CTRW for which long stalling periods between successive jumps lead to the nonergodic behavior [27] (see also Ref. [9] and references therein). Using the renewal technique (Appendix B), we derive the exact expressions for the mean mixing and ergodicity estimators. In the limit of large ω , they do not vanish but converge to nontrivial limits:

$$\langle \hat{E}_\infty(n,N) \rangle \simeq \alpha - 1 + \frac{\sin(\pi\alpha)}{\pi\alpha(1+\alpha)} (1-n/N)^\alpha \times {}_2F_1(\alpha, \alpha+1; \alpha+2; 1-n/N), \quad (13)$$

$$\langle \hat{F}_\infty(n,N) \rangle \simeq \alpha - 1 + \frac{\sin(\pi\alpha)}{\pi\alpha(1+\alpha)} \frac{N}{n} \times \int_{1-n/N}^1 dx x^\alpha {}_2F_1(\alpha, \alpha+1; \alpha+2; x), \quad (14)$$

where $0 < \alpha < 1$ is the scaling exponent of CTRW, and ${}_2F_1(a,b;c;z)$ is the hypergeometric function. These expressions present one of the main analytical results of the paper. The estimators do not vanish even for infinitely long trajectories: $\langle \hat{E}_\infty(n,\infty) \rangle = \langle \hat{F}_\infty(n,\infty) \rangle = \alpha$, independently of n . In sharp contrast to ergodic processes, the mean mixing estimator decreases from α to $\alpha - 1$ when n varies from 0 to N [Fig. 1(a)]. The longer the trajectory (larger N), the closer the numerical curves to the limiting Eqs. (13) and (14). Figures 1(b) and 1(d) show the standard deviations of both estimators that weakly depend on the trajectory length N , in contrast to Eq. (10) for discrete Gaussian processes. As a consequence, increasing N does not improve the estimation quality in the case of nonergodic CTRW.

C. Measurement noise and practical issues

Since both estimators vanish in the limit $\omega \rightarrow \infty$ for mixing and ergodic processes but remain nonzero for nonergodic CTRW, the estimation at very large ω might be thought as optimal. However, this strategy is not convenient in practice because of measurement artifacts such as localization errors, blurring, or electronic noises [28,29]. To account for some of these effects, the intrinsic trajectory $X(t)$ can be superimposed

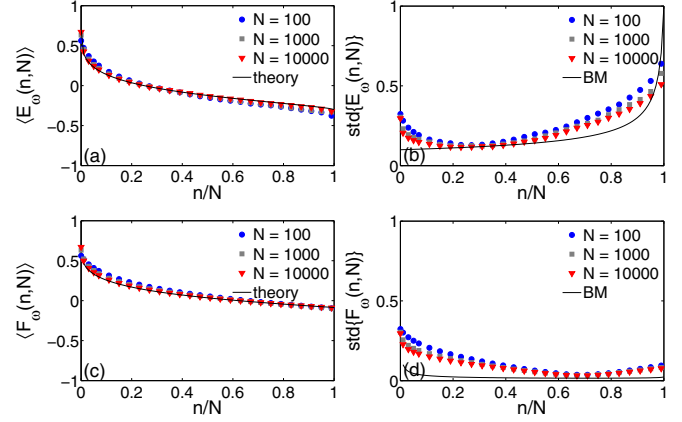


FIG. 1. The mean (a, c) and standard deviation (b, d) of the mixing (a, b) and ergodicity (c, d) estimators at $\omega = 10$ as a function of n/N for CTRW with $\alpha = 0.7$, $\sigma = 1$, and three trajectory lengths $N = 100, 1000, 10\,000$ (symbols). For comparison, solid line shows the theoretical limits (13) and (14) of the mean estimators for CTRW and the standard deviation for Brownian motion (given by square roots of Eqs. (11) and (12) with $N = 100$).

with a measurement noise $\epsilon(t)$: $\tilde{X}(t) = X(t) + \epsilon(t)$. If $\epsilon(t)$ is a white Gaussian noise independent of the tracer's dynamics $X(t)$, two contributions are factored out:

$$\langle e^{i\omega[\tilde{X}(n+k) - \tilde{X}(k)]} \rangle = \langle e^{i\omega[X(n+k) - X(k)]} \rangle e^{-\sigma_\epsilon^2 \omega^2}, \quad (15)$$

where the second factor is the average over the white noise of variance σ_ϵ^2 (when the measurement noise is not Gaussian, its effect onto the estimators can be different and needs further analysis). Even if the intrinsic dynamics is not mixing or ergodic, both estimators will be strongly attenuated in the limit of large ω by the second factor coming from the ergodic white noise. This is illustrated on Fig. 2, which shows the mean mixing estimator as a function of frequency ω for a CTRW corrupted by white Gaussian noise with different σ_ϵ . When there is no noise ($\sigma_\epsilon = 0$), the mean estimator rapidly saturates on a plateau, in agreement with the above theoretical analysis.

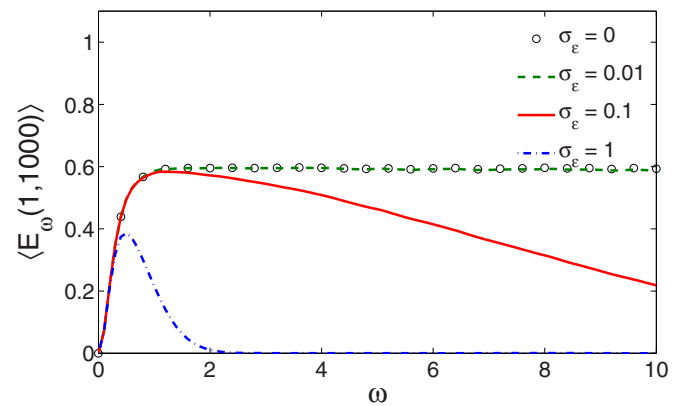


FIG. 2. The mean mixing estimator ($\langle \hat{E}_\omega(1,1000) \rangle$) as a function of ω for CTRW with $\alpha = 0.7$ and $\sigma = 1$, and four levels of white Gaussian noise: $\sigma_\epsilon = 0$ (circles) and $\sigma_\epsilon = 0.01, 0.1, 1$ (lines). Note that the plateau at 0.6 is smaller than the value $\alpha = 0.7$ expected from Eq. (13) because of the finite length effect ($N = 1000$).

In turn, the presence of noise attenuates the estimator. This effect is not yet seen at $\sigma_\varepsilon = 0.01$ because the factor $e^{-\omega^2\sigma_\varepsilon^2}$ remains close to 1 for the considered range of ω , but it is clearly seen for $\sigma_\varepsilon = 0.1$ and $\sigma_\varepsilon = 1$.

To limit this noise-induced attenuation, the rule of thumb consists in keeping $\omega\sigma$ of the order of 1, σ being the empirical standard deviation of increments. In practice, one can renormalize the trajectory by σ and then consider ω between 1 and 3. On one hand, this renormalization helps to eliminate false nonergodicity identifications due to too small σ . On the other hand, if the noise level σ_ε is much smaller than σ , the condition $\omega\sigma \sim 1$ ensures that the estimator is not much attenuated due to noise (i.e., the factor $e^{-\sigma_\varepsilon^2\omega^2}$ remains close to 1). At the same time, one can construct counterexamples for which this normalization is not enough. For instance, the trajectory concatenating two Brownian motions with different diffusion coefficients can be made appearing as nonergodic (Appendix C). Extending this construction to diffusion in a heterogeneous medium consisting of regions of random sizes and random diffusivities, one can produce a truly nonergodic process under simple assumptions on the distribution of the sizes and diffusivities [30,31].

D. Validation on anomalous diffusion models

In order to validate the proposed statistical tool, we apply the mixing and ergodicity estimators to four single trajectories generated according to four anomalous diffusion models with the same exponent $\alpha = 2H = 0.7$: fBm, CTRW, sBm, and diffusion on percolating cluster (in the last case, the exponent is random and distributed around 0.7 due to the random shape of percolating clusters; see Appendix D for details). Each trajectory is generated with the same one-step variance $\sigma^2 = 1$. To render the comparison closer to the experimental situation, all trajectories were corrupted by white Gaussian noise with standard deviation $\sigma_\varepsilon = 0.2$. Figure 3 shows four simulated trajectories and the corresponding curves of the mixing and ergodicity estimators. One can clearly distinguish the nonmixing feature of a CTRW trajectory even from noisy curves of the mixing estimator. These curves allow one to reject the mixing hypothesis with a high degree of certainty. Similarly, the nonergodic behavior is seen from the ergodicity estimator. In turn, the estimator curves for three other trajectories vanish as n increases so that the mixing and ergodicity hypotheses cannot be rejected. However, it does not imply mixing or ergodicity for these models. This is well illustrated by the scaled Brownian motion which is not ergodic, although its ergodicity estimator vanishes with n . The “mild nonergodicity” of this process is not detected by both estimators due to a relatively short trajectory length. This is not surprising because the one-step standard deviation varies from 1 at $n = 1$ to $500^{(\alpha-1)/2} \approx 0.4$ at $n = 500$. To detect the nonergodic behavior of this model, one needs higher variations and thus much longer trajectories.

To illustrate the statistical variability of estimators, we repeat the same analysis for ten simulated trajectories for each model. Note that Janczura and Weron have managed to reveal the ergodic property of fBm from empirical ensemble averages over many trajectories (the smallest analyzed sample containing ten trajectories) [15]. Here, we aim at probing

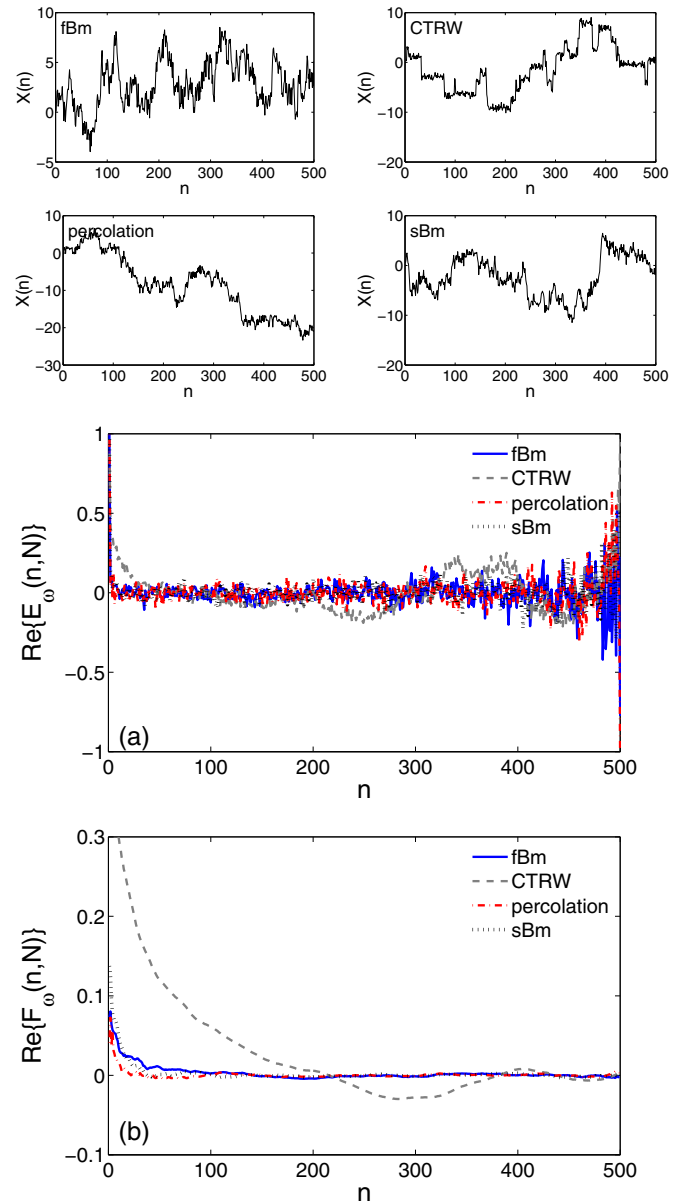


FIG. 3. (Top) Examples of trajectories of four anomalous diffusion models: fBm, CTRW, diffusion on percolating clusters, and sBm, with the same scaling exponent $\alpha = 0.7$ and one-step size $\sigma = 1$. Each trajectory was corrupted by the white Gaussian noise of level $\sigma_\varepsilon = 0.2$ and then renormalized by the empirical standard deviation of its increments. (Bottom) The real part of the mixing and ergodicity estimators at $\omega = 2$ applied to these four trajectories.

nonergodicity *individually* for each single trajectory. Figure 4 shows the results for the mixing estimator (only for fBm and CTRW), while the ergodicity estimator is illustrated in Fig. 5. Both estimators allow one to clearly identify the nonergodic character of CTRW from a single trajectory, even for the trajectory length as small as $N = 500$. Since the ergodicity estimator yields much smoother curves, it is more appropriate for the analysis of single-particle tracking experiments (note that although mixing and ergodicity are not equivalent, they are satisfied or violated simultaneously in many diffusive processes).

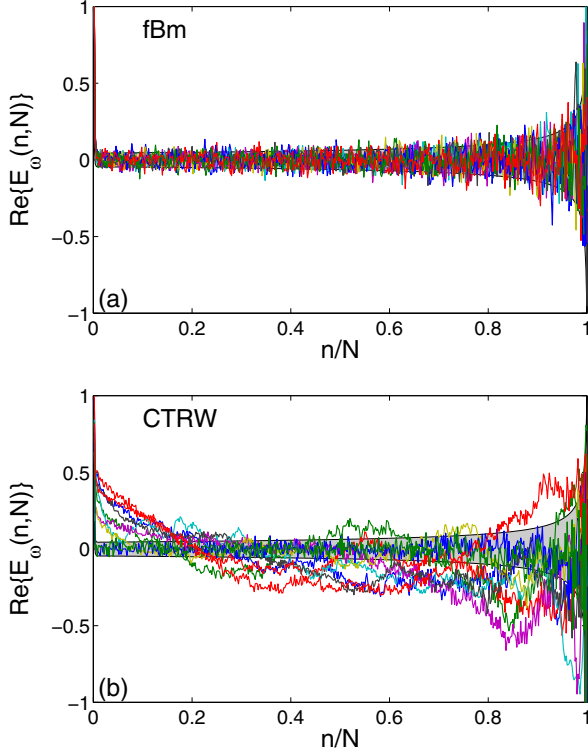


FIG. 4. The real part of the mixing estimator at $\omega = 2$ for ten simulated trajectories from two anomalous diffusion models: ergodic fBm with $2H = 0.7$ (a) and nonergodic CTRW with the same exponent $\alpha = 0.7$ (b) (in both cases, we set $\sigma = 1$ and $N = 500$). All trajectories were corrupted by white Gaussian noise with standard deviation $\sigma_\varepsilon = 0.1$. Each trajectory is renormalized by the empirical standard deviation of its increments. Light-gray shadowed region delimits the typical range of fluctuations for Brownian motion, i.e., the mean plus and minus the standard deviation.

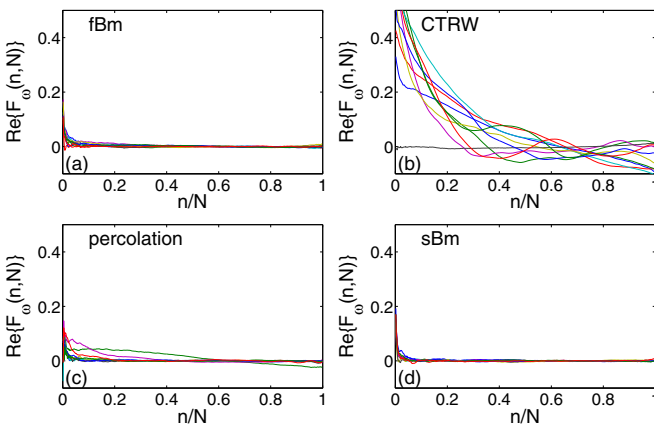


FIG. 5. The real part of the ergodicity estimator at $\omega = 2$ for ten simulated trajectories from four anomalous diffusion models with the same exponent $\alpha = 2H = 0.7$: fBm (a), CTRW (b), diffusion on percolating cluster (c), and sBm (d) (in all cases, we set $\sigma = 1$ and $N = 500$). All trajectories were corrupted by white Gaussian noise with standard deviation $\sigma_\varepsilon = 0.1$. Each trajectory was renormalized by the empirical standard deviation of its increments.

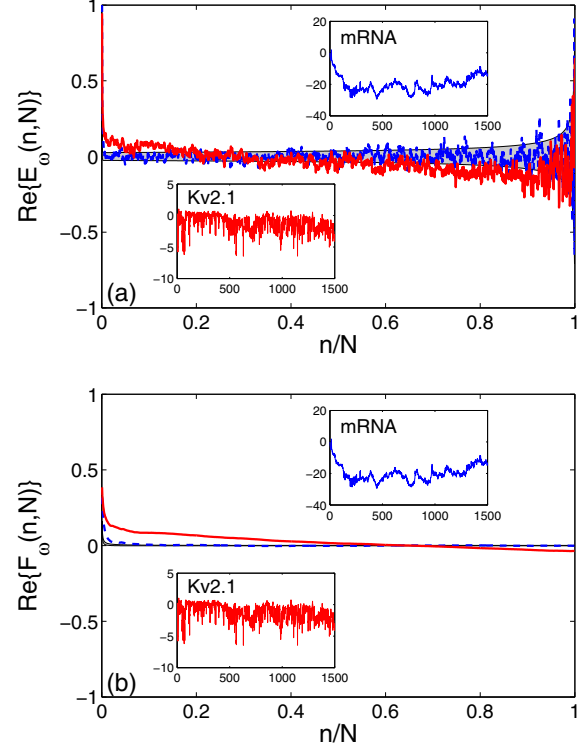


FIG. 6. The real part of the mixing (a) and ergodicity (b) estimators at $\omega = 2$ as a function of n for two experimental trajectories of around $N = 1500$ points: the motion of mRNA molecule inside live *E. coli* cell [33] and Kv2.1 potassium channel anomalous dynamics in the plasma membrane [1]. Both trajectories (shown in insets) were renormalized by the empirical standard deviation of their increments. Light-gray shadowed region delimits the typical range of fluctuations of estimators for Brownian motion, i.e., the mean plus and minus the standard deviation.

In addition, both estimators were also successfully tested on CTRW with exponential cutoff, which allows one to “switch” between ergodic and nonergodic behavior (Appendix D 3), and on the nonergodic geometric Brownian motion (Appendix D 4) that plays a major role in finances [26,32].

E. Application to experimental data

Now, we apply both estimators to two samples of experimental trajectories: (i) mRNA molecules inside live *Escherichia coli* cells [33], and (ii) Kv2.1 potassium channels in the plasma membrane [1]. Figure 6(a) shows that the mixing estimator applied to a trajectory of mRNA molecule (dashed line) rapidly decreases with n and then fluctuates around 0 within the typical range of fluctuations for Brownian motion. In other words, this test does not reveal nonmixing behavior, in agreement with conclusion of Ref. [14]. Similarly, the ergodicity estimator in Fig. 6(b) rapidly vanishes at large n , as expected for ergodic dynamics. However, many trajectories are needed to confirm that the dynamics is indeed mixing or ergodic (see further discussion in Sec. IV). In turn, both mixing and ergodicity estimators for a trajectory of the Kv2.1 potassium channel (solid line) lie outside the typical range and do not vanish as n increases. This is a signature of the

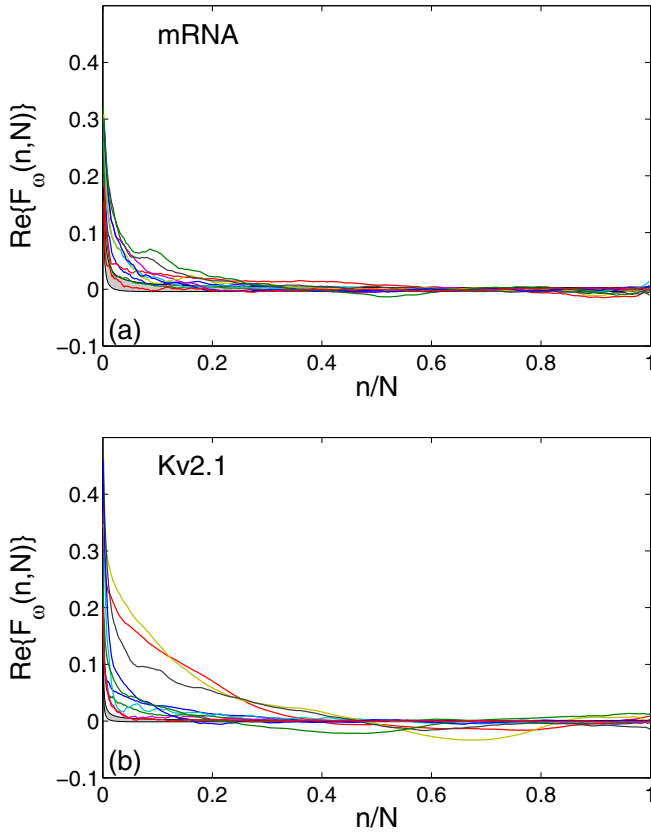


FIG. 7. The real part of the ergodicity estimator at $\omega = 2$ for ten experimental trajectories of two samples: the motion of mRNA molecules inside live *E. coli* cells [33] and Kv2.1 potassium channel anomalous dynamics in the plasma membrane [1]. Each trajectory is renormalized by the empirical standard deviation of its increments. The trajectory length ranges between 400 and 500 points for the first set and around 1500 points for the second set. Light-gray shadowed region delimits the typical range of fluctuations for Brownian motion, i.e., the mean plus and minus the standard deviation.

nonmixing and nonergodic behavior, in agreement with the conclusion of Weigel *et al.* based on the analysis of ensemble averages over multiple trajectories [1].

We also applied both estimators to the trajectories of optically trapped (sub)micron-sized beads in living cells and actin solutions [34,35]. These tests (not shown) did not reveal nonergodic behavior, as expected for a harmonically trapped particle.

The important advantage of these single-particle estimators is the possibility to probe nonergodicity for each trajectory. Figure 7 shows the real part of the ergodicity estimator at $\omega = 2$ for ten experimental trajectories from two samples: the motion of mRNA molecules inside live *E. coli* cells [33] and Kv2.1 potassium channel anomalous dynamics in the plasma membrane [1]. One can see that the dispersion of the estimator curves is higher for the Kv2.1 potassium channel, in particular, several trajectories can be classified as nonergodic. As a consequence, the ergodicity estimator allows one to reject, with some degree of certainty, the ergodicity hypothesis. Weigel *et al.* identified transient binding to the actin cytoskeleton as a plausible biophysical origin of nonergodicity in this dynamics.

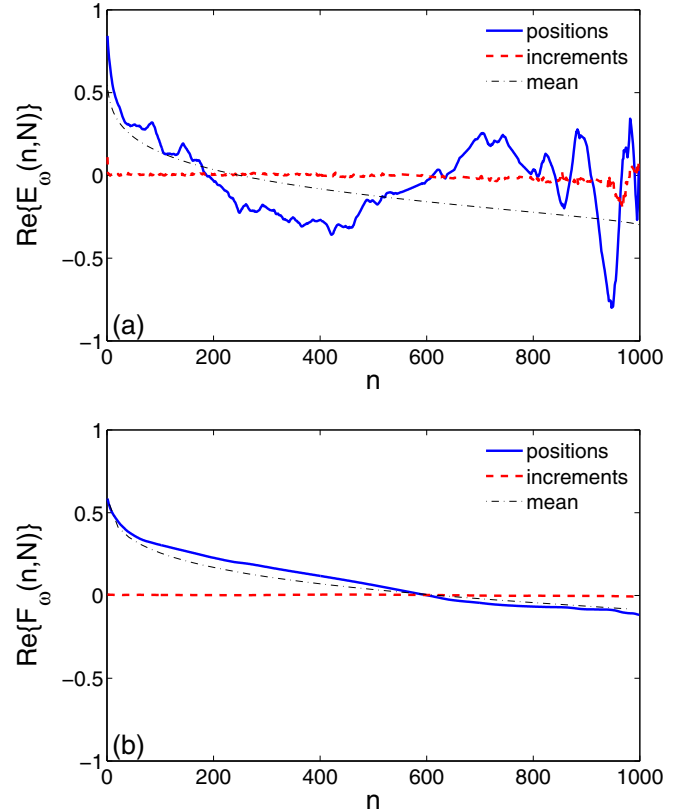


FIG. 8. The real parts of the mixing (a) and ergodicity (b) estimators at $\omega = 1$ applied to the increments of a single CTRW trajectory (dashed line) and to the positions of the same trajectory (solid line), with $N = 1000$, $\alpha = 0.7$, and $\sigma = 1$. In both cases, $X(n)$ are renormalized by the empirical standard deviation of the increments. Thin dash-dotted line presents the mean estimators from Eqs. (13) and (14).

In turn, the estimator curves for mRNA molecule trajectories are less dispersed and vanish as n grows, showing no evidence for nonergodic behavior.

It is also instructive to compare Fig. 7 to Fig. 5 for simulated trajectories. One can see that the ergodicity estimator curves for both experimental samples behave somewhat in between those for fBm and CTRW. In fact, their dispersion is larger than that for fBm but smaller than that for CTRW.

III. DISCUSSION

A. Positions versus increments

The forms of both mixing and ergodicity estimators originate from the analysis of stationary infinitely divisible (SID) processes by Magdziarz and Weron [14]. For instance, the mixing estimator aims at testing whether two increments $Y(k+n)$ and $Y(k)$ become asymptotically independent as n increases. However, the use of these short-time increments (or velocities) may be inconvenient for the analysis of anomalous intracellular transport because the most common nonergodic model of anomalous diffusion, the CTRW, cannot be classified as nonergodic since most of its increments are zero. Figure 8 illustrates this problem by comparing the increments-based

method (as originally proposed by Magdziarz and Weron) and the positions-based method (that we employ in this paper). For this purpose, we first apply the mixing and ergodicity estimators to the increments of a single CTRW trajectory, $\{X(1) - X(0), X(2) - X(1), \dots, X(N) - X(N-1)\}$, and then to the positions of the same trajectory, $\{X(0), X(1), \dots, X(N)\}$ (note that the improved estimators operate with long-time increments, namely, $X(k+n) - X(k)$ and $X(k) - X(0)$ stand in Eq. (3)). As expected, both original estimators applied to the short-time increments are very close to 0, which does not allow one to reveal its nonergodic character. In turn, the estimators applied to the positions of the same CTRW reveal its nonergodicity and nonmixing behavior. It is worth noting that the two methods can both work well (correctly identifying CTRW trajectories as nonergodic) or both fail (missing such identifications). This is related to the high sensitivity of the estimators to the presence of long stalling periods in a finite length trajectory. However, the use of the positions-based estimators results in statistically more reliable identifications of CTRW as nonergodic.

While we kept essentially the same form of both mixing and ergodicity estimators, their application to the positions of a trajectory has changed the theoretical paradigm. In particular, the improved mixing estimator probes now the asymptotic independence of the positions $X(k+n)$ and $X(k)$ or, equivalently, of the long-time increments $X(k+n) - X(0)$ and $X(k) - X(0)$ at different lag times. Alternatively, this estimator can be seen as the time averaged characteristic function of the increment $X(k+n) - X(k)$ at lag time n . In other words, the key modification consists in looking at the long-time increments instead of short-time ones [such as $X(k+1) - X(k)$]. To some extent, the difference between the increments-based and the positions-based estimators resembles the difference in estimation of the velocity autocorrelation function and the mean-square displacement, the latter being less noisy and thus more robust and easier to estimate.

To further illustrate the difference between two methods, we plot in Fig. 9 the real part of the original ergodicity estimator [14] applied to the increments of ten experimental trajectories of mRNA molecules and of Kv2.1 potassium channels [55]. Given that the mRNA and Kv2.1 trajectories were recorded in different length units, the increments of each trajectory were renormalized by their standard deviation. Following Ref. [14], only the first 200 lag times are plotted. One can see that the original estimators look very similar for two sets of experimental data, suggesting the ergodic behavior in both cases. In contrast, our improved estimator reveals more distinct behavior in two samples (Fig. 7).

B. Role of the frequency

The introduction of variable frequency ω is important to avoid wrong identifications of nonmixing or nonergodic behavior due to deviations of the mixing or ergodicity estimators from 0. This problem can be relevant for both the original increments-based method and our positions-based method. In order to illustrate this point, we consider two examples: fractional Gaussian noise (fGn) and Brownian motion.

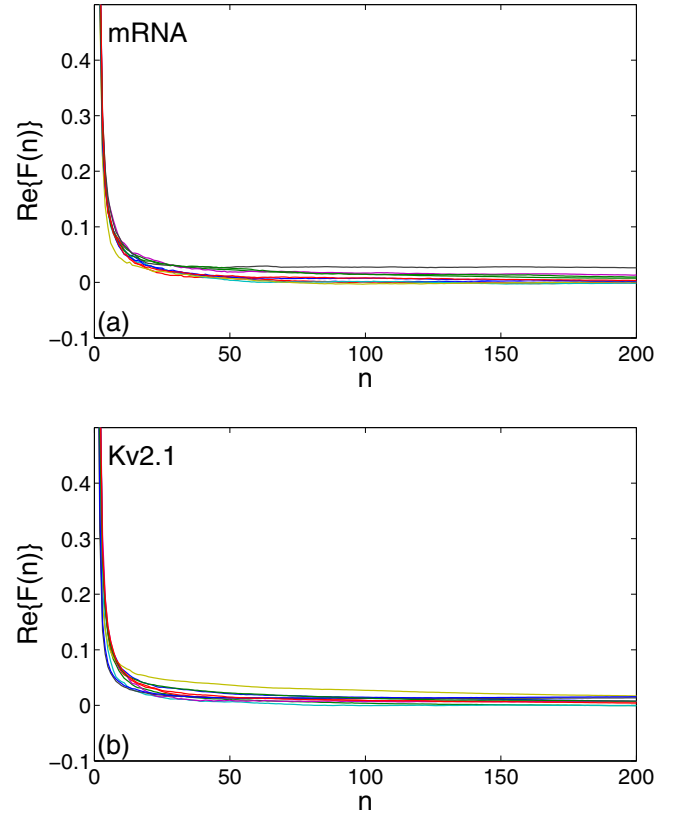


FIG. 9. The real part of the original ergodicity estimator, $\text{Re}\{n^{-1} \sum_{k=0}^{n-1} \hat{E}(k)\}$ from Ref. [14], applied to ten experimental trajectories of two samples: (a) the motion of mRNA molecules inside live *E. coli* cells [33] and (b) Kv2.1 potassium channel anomalous dynamics in the plasma membrane [1]. The estimator is applied to the increments of each trajectory, which are renormalized by their empirical standard deviation. The trajectory length ranges between 400 and 500 points for the first set and around 1500 points for the second set.

If $X(n)$ are centered stationary Gaussian increments defined by a covariance function $\langle X(k_1)X(k_2) \rangle = \gamma(|k_1 - k_2|)$, the mean mixing and ergodicity estimators read

$$\begin{aligned} \langle \hat{E}_\omega(n, N) \rangle &= e^{-\omega^2 \eta(n)} - 2 \sum_{k=1}^N \frac{N-k+1}{N(N+1)} e^{-\omega^2 \eta(k)}, \\ \langle \hat{F}_\omega(n, N) \rangle &= \frac{1}{n} \sum_{k=1}^n e^{-\omega^2 \eta(k)} - 2 \sum_{k=1}^N \frac{N-k+1}{N(N+1)} e^{-\omega^2 \eta(k)}, \end{aligned}$$

where $\eta(n) = \gamma(0) - \gamma(n)$. For instance, if $X(n)$ are the increments of fractional Brownian motion (the so-called fractional Gaussian noise), one has

$$\gamma(n) = \frac{\sigma^2}{2} [|n-1|^{2H} + (n+1)^{2H} - 2n^{2H}]. \quad (16)$$

For $H = 1/2$, one retrieves the discrete white noise with $\gamma(n) = \sigma^2 \delta_{n,0}$ that implies $\langle \hat{E}_\omega(n, N) \rangle = \langle \hat{F}_\omega(n, N) \rangle = 0$. More generally, both mean estimators are strictly zero for independent $X(n)$.

In turn, for correlated increments, the original estimators at $\omega = 1$ can deviate from 0 even for ergodic processes. Figure 10

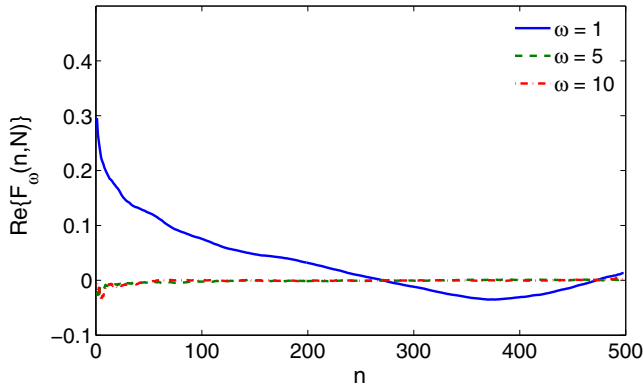


FIG. 10. The real part of the ergodicity estimator as a function of n for a single fGn trajectory with $N = 500$, $H = 0.9$, and $\sigma = 1$. At $\omega = 1$ (solid line), the estimator deviates from zero that may wrongly suggest nonergodic behavior. Increasing ω , one can eliminate this false conclusion.

shows the real part of the ergodicity estimator for a single realization of ergodic fGn. At $\omega = 1$, the estimator deviates from zero that may wrongly be interpreted as nonergodic behavior. Increasing the frequency ω allows one to re-establish the vanishing behavior of the estimator and thus to avoid such false conclusions. While the deviations are relatively small for the considered case of fGn (and are even smaller for other choices of H and σ), they could be stronger for some other ergodic processes. In general, the frequency ω is needed to control the amplitude of increments.

The effect of amplitude can be much more important when the estimators are applied to the positions of a trajectory instead of its increments. In particular, even Brownian motion can be falsely identified as nonergodic if the diffusion coefficient is small. This statement is illustrated on Fig. 11, which shows the mean mixing and ergodicity estimators as well as the real part

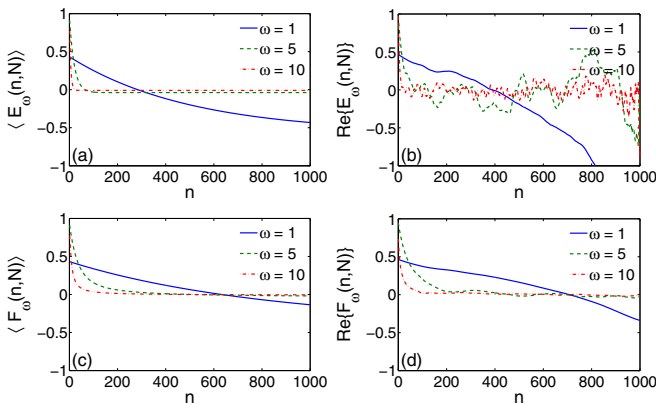


FIG. 11. The mean mixing (a) and ergodicity (c) estimators as a function of n for a Brownian motion trajectory with $N = 1000$ and $\sigma^2 = 0.04$. At $\omega = 1$ (solid line), both estimators are not small that may wrongly suggest nonmixing or nonergodic behavior. Increasing ω , one can eliminate this false conclusion. The same conclusions can be made from the real part of the mixing (b) and ergodicity (d) estimators for a single Brownian motion trajectory with the same parameters.

of both estimators for a single Brownian motion trajectory with $N = 1000$ and $\sigma^2 = 0.04$. Distinct deviations from 0 are clearly seen at $\omega = 1$. This is a finite-length effect that would disappear for a much longer trajectory. For a fixed N , this false conclusion can be removed by increasing ω , which is equivalent to rescaling the variance σ^2 . In practice, we suggest renormalizing the trajectory by the empirical standard deviation of its increments, in which case the frequency ω can be kept in the order of 1.

C. Impact of outliers

In addition to noise, experimental data can contain “outliers,” i.e., singular erroneous points coming from instrumental or software failures, data recording or transmission problems, or human factors. The problem of outliers is particularly relevant for financial data [36]. These erroneous points whose statistical properties strongly deviate from the remaining “normal” points, may appear as nonergodic features in the analysis of a single finite length trajectory by means of the mixing and ergodicity estimators. In order to illustrate the potential impact of outliers, we generate a Brownian trajectory with

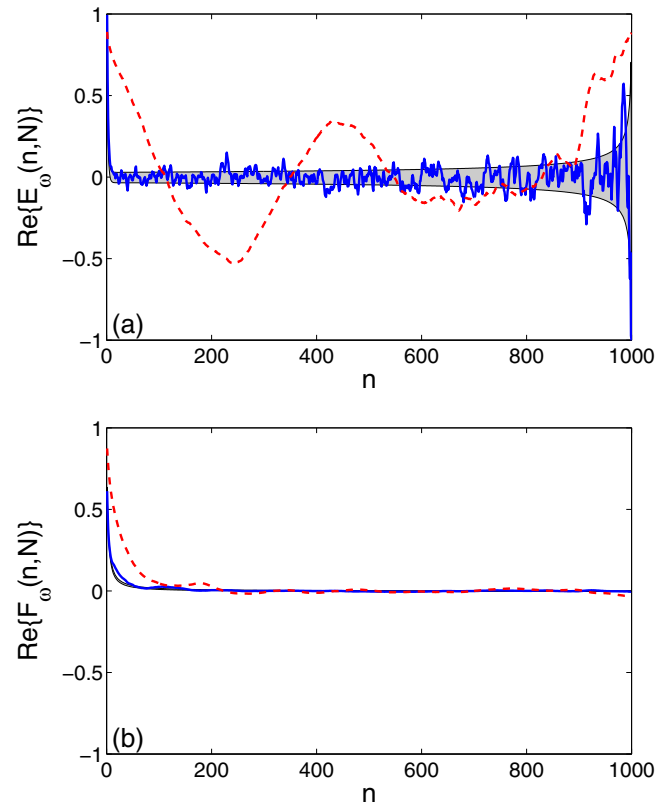


FIG. 12. The real part of the mixing (a) and ergodicity (b) estimators at $\omega = 1$ as a function of n for an original Brownian motion trajectory with $N = 1000$ and $\sigma = 1$ (solid line) and for the same trajectory corrupted by resetting ten randomly chosen points to 0 (dashed line). In both cases, the trajectory was renormalized by the empirical standard deviation of its increments. Light-gray shadowed region delimits the mean plus and minus the standard deviation of each estimator computed for Brownian motion according to Eqs. (8), (9), and (11).

$N = 1000$ steps and then reset 10 randomly chosen points of this trajectory to 0. This procedure results in 20 increments of anomalously large amplitude (as compared to the other increments). While only 1% of data points are assigned as outliers, both mixing and ergodicity estimators suggest nonmixing and nonergodic behavior, as illustrated on Fig. 12.

D. Discrete displacements

Digital acquisition systems or lattice models can produce discretely spaced positions of experimental or simulated trajectories, resulting in a periodic (nonvanishing) behavior of both estimators as functions of the frequency ω . To illustrate this “artifact,” we consider the one-dimensional projection of a d -dimensional random walk in which $X(n)$ is the sum of independent random variables χ_k taking the values $\pm\sigma$ with probability $1/(2d)$, or 0 with probability $1 - 1/d$. For this process, $\langle e^{i\omega(X(n+k) - X(k))} \rangle = [\phi(\omega)]^n$, where $\phi(\omega)$ is the characteristic function of χ_k : $\phi(\omega) = 1 - (1 - \cos(\omega\sigma))/d$. The mean mixing and ergodicity estimators are still given by Eqs. (8) and (9), with $q = \phi(\omega)$. One can see that both mean estimators are 2π -periodic functions of $\omega\sigma$. As a consequence, too large values of $\omega\sigma$ do not improve the quality of estimation. Moreover, the estimators would lead to false nonmixing or nonergodicity identifications at the values $\omega\sigma = 2\pi m$ (with an integer m), at which $q = 1$. In turn, there is an optimal value minimizing q , which corresponds to $\omega\sigma = \pi/2 \simeq 1.57$ for this model. Note that if the trajectory was renormalized by the standard deviation of its increments, σ/\sqrt{d} , the characteristic function would be $\phi(\omega) = 1 - (1 - \cos(\omega/\sqrt{d}))/d$, and the optimal value would be $\omega = \sqrt{d}\pi/2$. Since the underlying model is not known for experimental data, the rule of thumb consists in analyzing the estimators for several values of ω in the range between 1 and 3.

IV. CONCLUSIONS

In summary, we proposed, investigated, and validated the improved mixing and ergodicity estimators based on long-time increments (or positions) of a single trajectory. Aiming applications to experimental trajectories, which *a priori* are neither stationary nor infinitely divisible, we extended the range of applicability of the estimators beyond SID processes. The new estimators rely on the time-averaged characteristic function of the increments that can bring complementary information as compared to the time-averaged MSD or VAF, especially for non-Gaussian processes. We showed that the ergodicity estimator vanishes for basic ergodic models of anomalous diffusion (fBm, diffusion on fractals) and remains nonzero for nonergodic models (CTRW, geometric Brownian motion). The significant advantage of the present method is that nonmixing or nonergodic behavior can be revealed from a single trajectory, with no need in ensemble averages over many trajectories that may be difficult or even impossible to collect.

As discussed by Magdziarz and Weron [14], the smallness of the estimators is the necessary but not sufficient condition for mixing and ergodicity. In other words, these statistical tests can reveal nonmixing or nonergodic properties from a single trajectory but many trajectories are needed to confirm mixing

or ergodicity. For instance, a constant process $X(n) = x_0$ with a random initial position x_0 is not ergodic, and this property cannot in principle be revealed from a single trajectory. In particular, the mixing and ergodicity estimators are strictly zero for this process but their smallness is not a signature of ergodicity but rather a failure in detecting nonergodicity. The scaled Brownian motion is another example of such a failure. In general, the finite trajectory length and the randomness of the estimators based on a single trajectory remain the major challenges for inference problems that aim at characterizing an unknown stochastic process from its single random realization. Deviations of the estimators from 0 can be either a signature of nonmixing or nonergodic behavior, or a sign of nonstationary dynamics, or a consequence of too short trajectory, or a measurement artifact (e.g., the presence of outliers; see Sec. III C), or a specific feature of the process (e.g., discrete displacements; see Sec. III D).

While probing nonergodicity of an unknown stochastic process from a single finite length trajectory remains debatable from the mathematical point of view, the ergodicity and mixing estimators answer the important practical question whether the time average along a single trajectory is representative or not. If the estimators do not vanish with the lag time n , conclusions based on time averages can be strongly misleading. In particular, large values of the estimators indicate on peculiar properties of the stochastic process that should warn scientists against a blind use of time averages. Along with other single-particle methods [9,37–48], the mixing and ergodicity estimators provide a powerful statistical tool for a more reliable interpretation of SPT experiments.

An important perspective of this work consists in formulating nonergodicity and nonmixing test statistics (that can be converted to an estimated yes or no answer) and in quantifying their properties (p values, confidence intervals, etc.). For this purpose, the probability distribution of the estimators need to be investigated for various stochastic processes. In addition, the role of small sample statistics can be analyzed for the improved estimators (see Ref. [15] for details).

ACKNOWLEDGMENTS

The authors acknowledge the support under Grant No. ANR-13-JSV5-0006-01 of the French National Research Agency. We thank Dr. I. Golding and Dr. D. Krapf who provided experimental trajectories from their earlier publications.

APPENDIX A: VARIANCE OF THE ESTIMATORS

For a discrete centered Gaussian process, the variance Eq. (10) of the mixing estimator can be formally expressed in terms of the covariance matrix, with

$$\langle \hat{E}_\omega(n, N) \rangle = \frac{1}{N - n + 1} \sum_{k=0}^{N-n} C_{k+n, k, 0, 0} - \frac{1}{N(N+1)} \sum_{k_1 \neq k_2=0}^N C_{k_1, k_2, 0, 0} \quad (\text{A1})$$

and

$$\begin{aligned} & \langle |\hat{E}_\omega(n, N)|^2 \rangle \\ &= \frac{1}{(N-n+1)^2} \sum_{k, k'=0}^{N-n} C_{k+n, k, k'+n, k'} \\ & \quad - \frac{2}{(N-n+1)N(N+1)} \sum_{k=0}^{N-n} \sum_{k_1 \neq k_2=0}^N C_{k+n, k, k_1, k_2} \\ & \quad + \frac{1}{N^2(N+1)^2} \sum_{k_1 \neq k_2, k_3 \neq k_4}^N C_{k_1, k_2, k_3, k_4}, \end{aligned} \quad (\text{A2})$$

where

$$C_{k_1, k_2, k_3, k_4} = e^{-\frac{1}{2}\omega^2((X(k_1)-X(k_2))-X(k_3)+X(k_4))^2} \quad (\text{A3})$$

includes the elements of the covariance matrix. Even for Brownian motion, the combinatorial computation of all terms in Eq. (A2) is tedious while the formulas are cumbersome. It is more instructive to investigate the variance in the limit $\omega \rightarrow \infty$, in which only the terms $C_{k, k, k', k'} = C_{k, k', k, k'} = 1$ do not vanish exponentially. Keeping only these terms, one easily finds

$$\text{var}\{\hat{E}_\infty(n, N)\} = \frac{1}{N-n+1} - \frac{1}{N(N+1)}. \quad (\text{A4})$$

The variance is of the order of $1/N$ for small n but progressively grows up to 1 at $n = N$. For long trajectories ($N \gg 1$), the second term can be neglected.

The same technique yields the large ω asymptotic behavior of the variance of the ergodicity estimator:

$$\text{var}\{\hat{F}_\infty(n, N)\} = \frac{1}{n^2} \sum_{k=1}^n \frac{1}{N-k+1} - \frac{1}{N(N+1)}, \quad (\text{A5})$$

in which the second term can be neglected for $N \gg 1$.

For the case of Brownian motion, Fig. 13 illustrates how the standard deviation of the mixing and ergodicity estimators approaches their asymptotic limits [given by square roots of Eqs. (A4) and (A5)] as ω increases. One can see that the asymptotic formulas become accurate approximations for $\omega\sigma \gtrsim 2$.

APPENDIX B: CONTINUOUS-TIME RANDOM WALKS

We consider the continuous-time random walks with independent centered Gaussian jumps of variance σ^2 , separated by independent waiting times with a prescribed probability density $\psi(t)$. Throughout this Appendix, we use the continuous-time version of the estimators, in which k, n , and N are placed by t, Δ , and T , respectively:

$$\begin{aligned} \hat{E}_\omega(\Delta, T) &= \frac{1}{T-\Delta} \int_0^{T-\Delta} dt e^{i\omega[X(t+\Delta)-X(t)]} \\ & \quad - \frac{1}{T^2} \int_0^T dt_1 \int_0^T dt_2 e^{i\omega[X(t_1)-X(t_2)]}. \end{aligned} \quad (\text{B1})$$

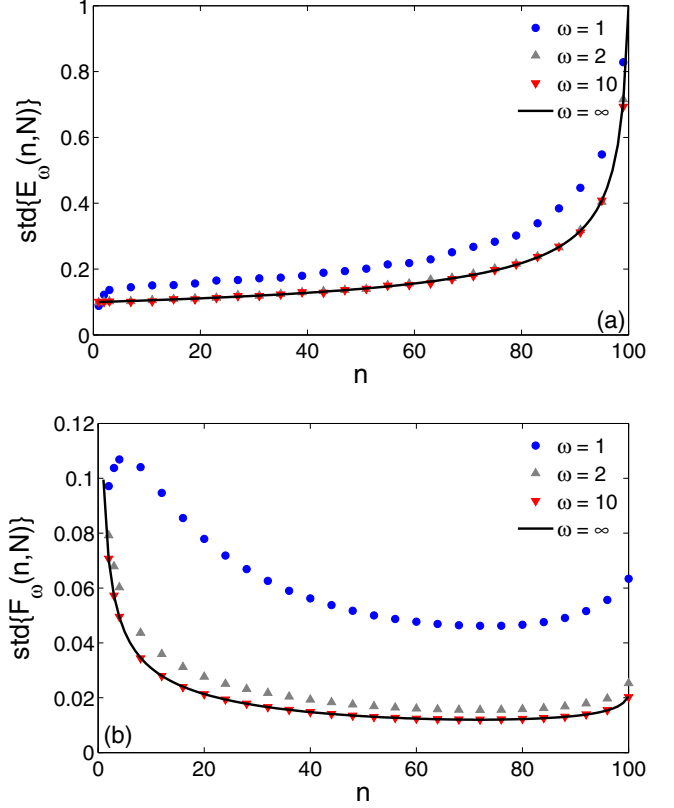


FIG. 13. The standard deviation of the mixing (a) and ergodicity (b) estimators at several values of ω for Brownian motion with $N = 100$ and $\sigma = 1$. The large ω asymptotic limits given by square roots of Eqs. (11) are shown by solid lines.

In order to obtain the mean $\langle \hat{E}_\omega(\Delta, T) \rangle$, one needs to compute the expectation

$$h_\omega(t, \Delta) \equiv \langle e^{i\omega[X(t+\Delta)-X(t)]} \rangle. \quad (\text{B2})$$

The mean mixing estimator can then be expressed as

$$\begin{aligned} \langle \hat{E}_\omega(\Delta, T) \rangle &= \frac{H_\omega(T-\Delta, \Delta)}{T-\Delta} \\ & \quad - \frac{2}{T^2} \int_0^T d\Delta H_\omega(T-\Delta, \Delta), \end{aligned} \quad (\text{B3})$$

where

$$H_\omega(t, \Delta) = \int_0^t dt' h_\omega(t', \Delta). \quad (\text{B4})$$

Note that $H_\omega(T-\Delta, \Delta)/(T-\Delta)$ is the mean time-averaged characteristic function of increments of a CTRW.

For CTRWs, the expectation in Eq. (B2) includes the average over the jump distribution and the average over the waiting time distribution. The first average is elementary for a Gaussian jump distribution:

$$h_\omega(t, \Delta) = \langle e^{-\frac{1}{2}\omega^2\sigma^2\mathcal{N}(t, t+\Delta)} \rangle_\psi, \quad (\text{B5})$$

where $\mathcal{N}(t, t+\Delta)$ is the random number of jumps between times t and $t+\Delta$, and $\langle \dots \rangle_\psi$ denotes the average over waiting times. In other words, $h_\omega(t, \Delta)$ is the Laplace transform of the probability density of $\mathcal{N}(t, t+\Delta)$ with respect to $\frac{1}{2}\omega^2\sigma^2$.

1. Number of jumps

The further computation of the function $h_\omega(t, \Delta)$ relies on renewal techniques [23]. First, the joint probability $P_{k,n}(t, \Delta)$ for getting k jumps in the interval $(0, t)$ and $n > 0$ jumps in the interval $(t, t + \Delta)$ can be written as

$$\begin{aligned} P_{k,n}(t, \Delta) &= \int_0^t dt' \psi_k(t') \int_t^{t+\Delta} dt_1 \psi(t_1 - t') \\ &\quad \times \int_{t_1}^{t+\Delta} dt_2 \psi(t_2 - t_1) \dots \\ &\quad \times \int_{t_{n-1}}^{t+\Delta} dt_n \psi(t_n - t_{n-1}) \Psi_0(t + \Delta - t_n), \\ &= \int_0^t dt' \psi_k(t') \int_0^\Delta dt_1 \psi(t_1 + t - t') \\ &\quad \times \int_{t_1}^\Delta dt_2 \psi(t_2 - t_1) \dots \\ &\quad \times \int_{t_{n-1}}^\Delta dt_n \psi(t_n - t_{n-1}) \Psi_0(\Delta - t_n), \end{aligned} \quad (\text{B6})$$

where $\Psi_0(t)$ is the probability of no jump until time t , and $\psi_k(t)$ is the probability density for the k th jump at time t . The Laplace transform with respect to Δ yields

$$\begin{aligned} \tilde{P}_{k,n}(t, s) &\equiv \int_0^\infty d\Delta e^{-s\Delta} P_{k,n}(t, \Delta) \\ &= \int_0^t dt' \psi_k(t') \tilde{\psi}_{t-t'}(s) [\tilde{\psi}(s)]^{n-1} \frac{1 - \tilde{\psi}(s)}{s}, \end{aligned} \quad (\text{B7})$$

where

$$\tilde{\psi}_t(s) \equiv \int_0^\infty dt' e^{-st'} \psi(t' + t). \quad (\text{B8})$$

The second Laplace transform with respect to t yields

$$\begin{aligned} \tilde{\tilde{P}}_{k,n}(s', s) &\equiv \int_0^\infty dt e^{-s't} \tilde{P}_{k,n}(t, s) \\ &= [\tilde{\psi}(s')]^k \tilde{\tilde{\psi}}(s', s) [\tilde{\psi}(s)]^{n-1} \frac{1 - \tilde{\psi}(s)}{s}, \end{aligned} \quad (\text{B9})$$

where

$$\begin{aligned} \tilde{\tilde{\psi}}(s', s) &\equiv \int_0^\infty dt e^{-st} \int_0^\infty dt' e^{-t's'} \psi(t + t') \\ &= \frac{\tilde{\psi}(s) - \tilde{\psi}(s')}{s' - s}. \end{aligned} \quad (\text{B10})$$

For the special case $n = 0$, one gets

$$P_{k,0}(t, \Delta) = \int_0^t dt' \psi_k(t') \Psi_0(t + \Delta - t'), \quad (\text{B11})$$

from which

$$\begin{aligned} \tilde{\tilde{P}}_{k,0}(s', s) &= [\tilde{\psi}(s')]^k \tilde{\tilde{\Psi}}_0(s', s) \\ &= [\tilde{\psi}(s')]^k \frac{1}{ss'} \left[1 - \frac{s\tilde{\psi}(s') - s'\tilde{\psi}(s)}{s - s'} \right]. \end{aligned} \quad (\text{B12})$$

The average of the joint distribution $P_{k,n}(t, \Delta)$ over k yields the marginal distribution of n steps in the interval $(t, t + \Delta)$:

$$P_n(t, \Delta) \equiv \sum_{k=0}^\infty P_{k,n}(t, \Delta), \quad (\text{B13})$$

from which

$$\begin{aligned} \tilde{\tilde{P}}_0(s', s) &= \frac{1}{1 - \tilde{\psi}(s')} \frac{1}{ss'} \left[1 - \frac{s\tilde{\psi}(s') - s'\tilde{\psi}(s)}{s - s'} \right], \\ \tilde{\tilde{P}}_n(s', s) &= \frac{1}{1 - \tilde{\psi}(s')} \frac{\tilde{\psi}(s) - \tilde{\psi}(s')}{s' - s} [\tilde{\psi}(s)]^{n-1} \frac{1 - \tilde{\psi}(s)}{s}. \end{aligned} \quad (\text{B14})$$

As a consequence, one gets

$$\begin{aligned} \tilde{\tilde{h}}_\omega(s', s) &= \sum_{n=0}^\infty e^{-\frac{1}{2}\omega^2\sigma^2 n} \tilde{\tilde{P}}_n(s', s) = \frac{1}{ss'(e^{\frac{1}{2}\omega^2\sigma^2} - \tilde{\psi}(s))} \\ &\quad \times \left[1 - \tilde{\psi}(s) + \frac{e^{\frac{1}{2}\omega^2\sigma^2} - 1}{1 - \tilde{\psi}(s')} \left(1 - \frac{s\tilde{\psi}(s') - s'\tilde{\psi}(s)}{s - s'} \right) \right]. \end{aligned} \quad (\text{B15})$$

Setting $\omega = 0$, one retrieves the probability normalization: $\tilde{\tilde{h}}_0(s', s) = 1/(ss')$ from which $h_0(t, \Delta) = 1$, as expected. The generating function $\tilde{\tilde{h}}_\omega(s', s)$ can be used to compute the moments of $\mathcal{N}(t, t + \Delta)$.

To retrieve $h_\omega(t, \Delta)$, one needs to perform the double inverse Laplace transform. In general, the Laplace inversion has to be performed numerically. For the special case of the exponential waiting-time distribution, the inversion becomes simple. Setting $\psi(t) = e^{-t/\delta}/\delta$ so that $\tilde{\psi}(s) = 1/(1 + s\delta)$, one finds exactly

$$\tilde{\tilde{h}}_\omega(s', s) = \frac{1}{s'[s + (1 - e^{-\frac{1}{2}\omega^2\sigma^2})/\delta]}, \quad (\text{B16})$$

from which

$$h_\omega(t, \Delta) = \exp[-(1 - e^{-\frac{1}{2}\omega^2\sigma^2})\Delta/\delta]. \quad (\text{B17})$$

This function corresponds to the Poisson probability distribution of the number of jumps in the interval $(t, t + \Delta)$ that does not depend on t as expected:

$$P_n(t, \Delta) = e^{-\Delta/\delta} \frac{(\Delta/\delta)^n}{n!}. \quad (\text{B18})$$

2. Macroscopic limit

In the macroscopic limit of large t and Δ , the above expressions can be simplified by considering small s and s' . In general, the Laplace-transformed probability density $\tilde{\psi}(s)$ behaves as

$$\tilde{\psi}(s) \simeq 1 - (\delta s)^\alpha + \dots \quad (s \rightarrow 0), \quad (\text{B19})$$

where $0 < \alpha \leq 1$ is the scaling exponent, and δ is a timescale of one jump. This behavior incorporates both normal diffusion

($\alpha = 1$) with a finite mean waiting time δ and anomalous diffusion ($\alpha < 1$) with a heavy-tailed waiting-time density: $\psi(t) \simeq \frac{\delta^\alpha}{|\Gamma(-\alpha)|} t^{-1-\alpha}$ as $t \rightarrow \infty$. In the macroscopic limit, the variance σ^2 of one jump scales as $2D_\alpha \delta^\alpha$, where D_α is the generalized diffusion coefficient. As a consequence, $e^{\frac{1}{2}\omega^2\sigma^2} \simeq 1 + D_\alpha \omega^2 \delta^\alpha + \dots$. In the lowest order in δ , Eq. (B15) reads

$$\tilde{h}_\omega(s', s) \simeq \frac{1}{s'} \frac{s^{\alpha-1}}{D_\alpha \omega^2 + s^\alpha} + \frac{D_\alpha \omega^2 (s'^{\alpha-1} - s^{\alpha-1})}{s'^\alpha (s - s') (D_\alpha \omega^2 + s^\alpha)}. \quad (\text{B20})$$

In particular, the derivative with respect to $\frac{1}{2}\omega^2\sigma^2 = D_\alpha \delta^\alpha \omega^2$ yields the mean number of jumps,

$$\langle \tilde{\mathcal{N}}(s', s) \rangle \simeq \frac{s^{-\alpha} - s'^{-\alpha}}{s \delta^\alpha (s - s')}, \quad (\text{B21})$$

from which

$$\langle \mathcal{N}(t, t + \Delta) \rangle \simeq \frac{1}{\delta^\alpha} \int_0^\Delta dt' \frac{(t + t')^{\alpha-1}}{\Gamma(\alpha)} = \frac{(t + \Delta)^\alpha - t^\alpha}{\delta^\alpha \Gamma(\alpha + 1)}, \quad (\text{B22})$$

as expected.

For normal diffusion ($\alpha = 1$), the second term in Eq. (B20) vanishes while the double inverse Laplace transform of the first term yields

$$h_\omega(t, \Delta) \simeq \exp(-D_1 \omega^2 \Delta), \quad (\text{B23})$$

which approximates Eq. (B17) in the macroscopic limit.

In turn, when $\alpha < 1$, the dominant contribution comes from the second term of Eq. (B20), especially in the limit of large ω :

$$\tilde{h}_\infty(s', s) \simeq \frac{s'^{\alpha-1} - s^{\alpha-1}}{s'^\alpha (s - s')}. \quad (\text{B24})$$

Using the identity for the double Laplace transform,

$$\begin{aligned} \mathcal{L}_{s_1} \mathcal{L}_{s_2} \left\{ \int_0^{t_1} dt' f(t') g(t_1 - t' + t_2) \right\} \\ = \tilde{f}(s_1) \frac{\tilde{g}(s_2) - \tilde{g}(s_1)}{s_1 - s_2}, \end{aligned} \quad (\text{B25})$$

one can invert the above relation by setting $\tilde{f}(s) = s^{-\alpha}$ and $\tilde{g}(s) = s^{\alpha-1}$:

$$h_\infty(t, \Delta) \simeq \frac{\sin(\pi\alpha)}{\pi} \frac{{}_2F_1(\alpha, \alpha; \alpha + 1; (1 + \Delta/t)^{-1})}{\alpha(1 + \Delta/t)^\alpha}, \quad (\text{B26})$$

where the integral in Eq. (B25) was expressed in terms of the hypergeometric function ${}_2F_1(a, b; c; z)$:

$$\int_0^1 dx \frac{x^{b-1} (1-x)^{c-b-1}}{(1-zx)^a} = \frac{\Gamma(b)\Gamma(c-b)}{\Gamma(c)} {}_2F_1(a, b; c; z).$$

To compute $H_\infty(t, \Delta)$ (i.e., the integral of $h_\infty(t, \Delta)$ over t in Eq. (B4)), one can add the extra factor s'^{-1} to Eq. (B24) and

then again perform the Laplace inversion:

$$\begin{aligned} H_\infty(t, \Delta) &\simeq \int_0^t dt_1 \frac{t_1^\alpha}{\Gamma(\alpha + 1)} \frac{(t - t_1 + \Delta)^{-\alpha}}{\Gamma(1 - \alpha)} \\ &= t \frac{\sin(\pi\alpha)}{\pi\alpha} \frac{{}_2F_1(\alpha, \alpha + 1; \alpha + 2; (1 + \Delta/t)^{-1})}{(1 + \alpha)(1 + \Delta/t)^\alpha}, \end{aligned} \quad (\text{B27})$$

which gives the first term in Eq. (B3).

Using the formula 7.512.3 from Ref. [49] to integrate $H_\infty(T - \Delta, \Delta)$ over Δ , one shows that the second term in Eq. (B3) is equal to $1 - \alpha$. We obtain therefore the asymptotic limit of the mean mixing estimator as $\omega \rightarrow \infty$:

$$\begin{aligned} \langle \hat{E}_\infty(\Delta, T) \rangle &\simeq \alpha - 1 + \frac{\sin(\pi\alpha)}{\pi\alpha(1 + \alpha)} (1 - \Delta/T)^\alpha \\ &\quad \times {}_2F_1(\alpha, \alpha + 1; \alpha + 2; 1 - \Delta/T). \end{aligned} \quad (\text{B28})$$

This expression is one of the main analytical results of this paper. As expected for a nonergodic CTRW, the estimator does not vanish even for infinitely long trajectories. In fact, when $T \rightarrow \infty$, the last term approaches 1 so that $\langle \hat{E}_\infty(\Delta, \infty) \rangle = \alpha$, independently of Δ . The same limit is formally obtained as $\Delta \rightarrow 0$: $\langle \hat{E}_\infty(0, T) \rangle = \alpha$. In the opposite limit $\Delta \rightarrow T$, the last term vanishes, yielding the negative value $\alpha - 1$. In other words, when the lag time Δ varies from 0 to T , the mean mixing estimator decreases from α to $\alpha - 1$, in sharp contrast to the case of ergodic processes.

From Eq. (B28), one also deduces the asymptotic behavior of the mean ergodicity estimator,

$$\begin{aligned} \langle \hat{F}_\infty(\Delta, T) \rangle &\simeq \frac{1}{\Delta} \int_0^\Delta d\Delta' \langle \hat{E}_\infty(\Delta', T) \rangle \\ &= \alpha - 1 + \frac{\sin(\pi\alpha)}{\pi\alpha(1 + \alpha)} \frac{T}{\Delta} \\ &\quad \times \int_{1-\Delta/T}^1 dx x^\alpha {}_2F_1(\alpha, \alpha + 1; \alpha + 2; x). \end{aligned} \quad (\text{B29})$$

We recall that Eqs. (B28) and (B29) are derived in the macroscopic limit when Δ and T greatly exceed the time-step scale δ .

APPENDIX C: BROWNIAN MOTION WITH TWO DIFFUSION COEFFICIENTS

To illustrate the potential impact of time-dependent diffusion coefficient onto the mixing estimator, we consider the trajectory concatenating two Brownian trajectories with distinct diffusion coefficients D_1 and D_2 . In the discrete case, one can generate such a process by adding independent Gaussian variables with variance $\sigma_1^2 = 2D_1\delta$ up to the step $m - 1$, and then completing the second part by independent Gaussian variables with $\sigma_2^2 = 2D_2\delta$, $m - 1/2$ being the ‘‘border’’ between two parts. The computation of the mean mixing estimator is cumbersome but straightforward:

$$\langle \hat{E}_\omega(n, N) \rangle = \frac{S_1}{N - n + 1} - \frac{2S_2}{N(N + 1)}, \quad (\text{C1})$$

where

$$S_1 = \begin{cases} m \leq N/2 & \begin{cases} (m-n)p^n + (N+1-m-n)q^n + \frac{q(p^n-q^n)}{p-q} & (n < m), \\ q^n(N+1-n-m + \frac{q^{1-m}(p^m-q^m)}{p-q}) & (m \leq n \leq N-m), \\ p^m q^{n-m+1} \frac{1-(q/p)^{N+1-n}}{p-q} & (n > N-m), \end{cases} \\ m > N/2 & \begin{cases} (m-n)p^n + (N+1-m-n)q^n + \frac{q(p^n-q^n)}{p-q} & (n \leq N-m), \\ (m-n)p^n + qp^n \frac{1-(q/p)^{N+1-m}}{p-q} & (N-m < n < m), \\ p^m q^{n-m+1} \frac{1-(q/p)^{N+1-n}}{p-q} & (n \geq m), \end{cases} \end{cases}$$

$$S_2 = -(N+1) + \frac{m-(m+1)p+p^{m+1}}{(1-p)^2} + \frac{N-m+1-(N-m+2)q+q^{N-m+2}}{(1-q)^2} + \frac{q(1-p^m)(1-q^{N-m+1})}{(1-p)(1-q)}, \quad (C2)$$

with $p = e^{-\omega^2 \sigma_1^2 / 2}$ and $q = e^{-\omega^2 \sigma_2^2 / 2}$. The estimator vanishes as $\omega \rightarrow \infty$, as expected. Setting $m = 1$ (or $m = N + 1$), one retrieves the mean mixing estimator in Eq. (8) for Brownian motion.

However, renormalizing the process by the standard deviation of its increments does not resolve the problem of false nonmixing classifications. In fact, setting ω^2 to be the inverse of the variance of increments of the whole trajectory, $\omega^{-2} = \mu \sigma_1^2 + (1-\mu) \sigma_2^2$ (with $\mu = (m-1)/N$), yields

$$p = e^{-\frac{1}{2}[\mu+(1-\mu)\nu]^{-1}}, \quad q = e^{-\frac{1}{2}\nu[\mu+(1-\mu)\nu]^{-1}}, \quad (C3)$$

where $\nu = \sigma_2^2 / \sigma_1^2$. As a consequence, varying μ and ν , one can make p or q close enough to 1 so that the mixing estimator would not appear as small, wrongly suggesting nonmixing behavior (similar conclusion holds for nonergodicity).

APPENDIX D: SEVERAL MODELS OF ANOMALOUS DIFFUSION

In this Appendix, we describe the results of nonergodicity testing on several models of anomalous diffusion and on geometric Brownian motion.

1. Diffusion on percolating clusters

Anomalous diffusion on fractals, which can mimic a multiscale hierarchical structure of the medium, is a common model for interpreting single particle tracking experiments. In particular, diffusion on percolating clusters has numerous applications for modeling transport phenomena in porous media [50]. For illustrative purposes, we only consider two-dimensional percolating clusters on a square lattice at the critical threshold probability $p_c \approx 0.59 \dots$. These clusters are known to have the fractal dimension $d_f = 91/48 \approx 1.896 \dots$ and to yield the anomalous diffusion with $\alpha \approx 0.7$ [21,51]. To test the mixing and ergodicity estimators, we first generate 10 random clusters on a 1000×1000 square lattice and then simulate 1000 random walk trajectories of length $N = 500$ for each cluster. Figure 14 shows the mean mixing and ergodicity estimators obtained by averaging over 1000 trajectories, each curve representing the average over one cluster. These curves are almost indistinguishable, suggesting

a very weak dependence on the particular random realization of the cluster. Both estimators do not reveal nonmixing or nonergodic behavior as expected. A small bias (deviation

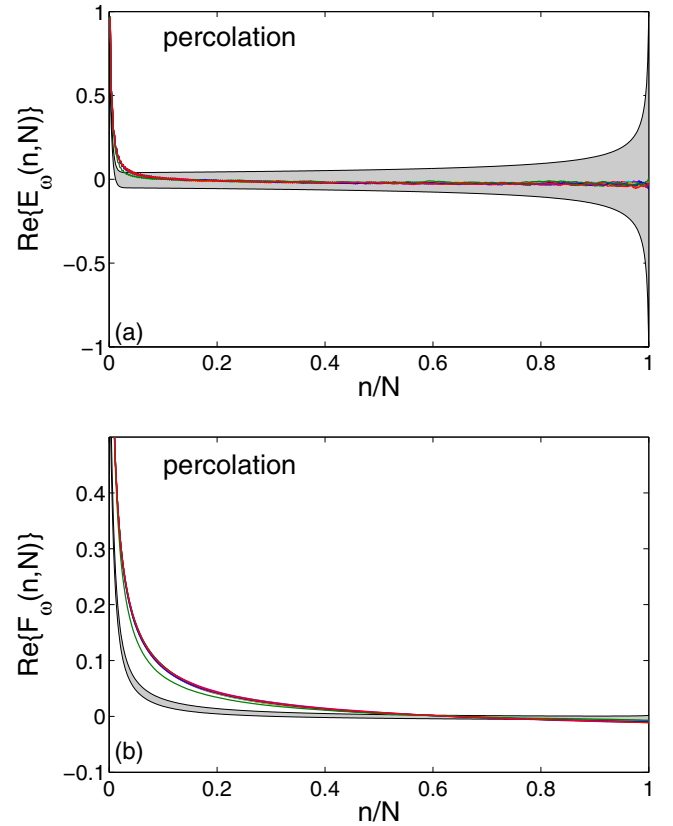


FIG. 14. The mean mixing (a) and ergodicity (b) estimators at $\omega = 1$ as a function of n for one coordinate $X(n)$ of two-dimensional random walk of length $N = 500$ on a critical percolating cluster on a 1000×1000 square lattice, with the lattice step $\sigma = 1$. Each curve presents the mean computed by averaging over 1000 trajectories generated on one cluster. The curves obtained for ten random clusters are almost identical. For comparison, light-gray shadowed region delimits the mean plus and minus the standard deviation of each estimator computed for Brownian motion according to Eqs. (8), (9), and (11).

from 0) at large n can be attributed to the relatively short trajectory length: the bias is reduced for longer trajectories (not shown).

2. Scaled Brownian motion

We also consider the scaled Brownian motion (sBm), a simple model of anomalous diffusion, in which the diffusion coefficient varies with time as $D(t) = \alpha D_\alpha t^{\alpha-1}$, where $0 < \alpha < 2$ is the scaling exponent, and D_α is the generalized diffusion coefficient [24,25]. This is a nonstationary Gaussian process obtained by rescaling Brownian motion $W(t)$: $X(t) = \sqrt{2D_\alpha} W(t^\alpha)$, for which $\langle [X(t_1) - X(t_2)]^2 \rangle = 2D_\alpha |t_1^\alpha - t_2^\alpha|$. The mean mixing estimator is then

$$\langle \hat{E}_\omega(n, N) \rangle = \frac{1}{N-n+1} \sum_{k=0}^{N-n} q^{(k+n)^\alpha - k^\alpha} - \frac{2}{N(N+1)} \sum_{k_1=0}^{N-1} \sum_{k_2=k_1+1}^N q^{k_2^\alpha - k_1^\alpha}, \quad (\text{D1})$$

where $q = e^{-\omega^2 \sigma^2 / 2}$ and $\sigma^2 = 2D_\alpha \delta^\alpha$, δ being the time step (the expression for the mean ergodicity estimator follows from its definition). In the limit of large $\omega\sigma$, both mean estimators vanish, showing no evidence for nonmixing or nonergodic behavior. At the same time, one can easily check that the ensemble averaged MSD, $\langle X^2(t) \rangle = 2D_\alpha t^\alpha$, differs from the time averaged MSD along the trajectory of length T ,

$$\frac{1}{T-t} \int_0^{T-t} dt_0 \langle [X(t_0+t) - X(t_0)]^2 \rangle \simeq 2D_\alpha T^{\alpha-1} t \quad (\text{D2})$$

(for $t \ll T$). In contrast to CTRW, this weak ergodicity breaking progressively vanishes as the trajectory length T (or N) goes to infinity [24,25]. Figuratively speaking, the scaled Brownian motion falls in between ergodic and nonergodic processes, with nonergodic features appearing only for finite length trajectories. The mixing and ergodicity estimators do not capture this peculiar behavior that illustrates their limitation.

3. CTRW with exponential cutoff

It is instructive to consider CTRW with exponential cutoff to “switch” between ergodic and nonergodic behavior. In order to simulate such CTRW trajectories, we generate random waiting times with the Pareto type III distribution defined by the cumulative function

$$F(t) = 1 - \left(1 + \frac{t}{\delta_s}\right)^{-\alpha} \exp\left(-\frac{t}{T_c}\right), \quad (\text{D3})$$

where δ_s is the time scale (fixed to be 1), α the scaling exponent, and T_c is the cutoff time. As discussed in Ref. [52], the cumulative function Eq. (D3) can be explicitly inverted to generate the waiting times τ from the uniformly distributed variable η ,

$$\tau = \alpha T_c W\left(\frac{\beta}{\alpha} e^{\beta/\alpha} (1-\eta)^{-1/\alpha}\right) - \delta_s, \quad (\text{D4})$$

where $\beta = \delta_s/T_c$, and $W(x)$ is the real branch of the Lambert function satisfying $W(x)e^{W(x)} = x$. In the limit $T_c \rightarrow \infty$

(no cutoff), one retrieves the standard Pareto waiting times generated as $\tau = \delta_s [(1-\eta)^{-1/\alpha} - 1]$.

The characteristic function and the moments of τ can be written as [52]

$$\langle e^{ik\tau} \rangle = 1 + ik\delta_s e^{\beta - ik\delta} (\beta - ik\delta)^{\alpha-1} \Gamma(1-\alpha, \beta - ik\delta),$$

$$\langle \tau^n \rangle = \delta_s^n e^\beta \sum_{j=1}^n \binom{n}{j} \frac{j(-1)^{n-j}}{\beta^{j-\alpha}} \Gamma(j-\alpha, \beta),$$

where $\Gamma(k, z)$ is the incomplete Γ function. In particular, the mean waiting time,

$$\langle \tau \rangle = \delta_s e^{\delta_s/T_c} (\delta_s/T_c)^{\alpha-1} \Gamma(1-\alpha, \delta_s/T_c), \quad (\text{D5})$$

asymptotically behaves as

$$\langle \tau \rangle \simeq \begin{cases} T_c (\delta_s/T_c)^\alpha \Gamma(1-\alpha), & (T_c \gg \delta_s), \\ T_c, & (T_c \ll \delta_s). \end{cases} \quad (\text{D6})$$

The generated sequence of waiting times, $\{\tau_k\}$, is then applied to produce positions of CTRW at equal time steps δ by assigning the same random position x_k to X_n over a time interval between $\tau_1 + \dots + \tau_k$ and $\tau_1 + \dots + \tau_k + \tau_{k+1}$,

$$X_n = \begin{cases} 0, & 0 \leq n\delta < \tau_1, \\ x_k, & \sum_{j=1}^k \tau_j \leq n\delta < \sum_{j=1}^{k+1} \tau_j, \end{cases} \quad (\text{D7})$$

where $x_k = x_{k-1} + \chi_k$, with χ_k being independent Gaussian displacements with mean zero and variance σ^2 .

Figure 15 shows the mean and standard deviation of the mixing and ergodicity estimators as a function of n computed numerically for CTRW with exponential cutoff. When the cutoff time T_c is significantly smaller than the trajectory length (here, $N = 1000$), the mean mixing estimator $\langle \hat{E}_\omega(n, N) \rangle$ vanishes very rapidly with n (dash-dotted line or circles), as expected for Brownian motion. In turn, for larger T_c , long waiting times break the ergodicity and mixing (dashed and solid lines or triangles). Note also that $\langle \hat{E}_\omega(n, N) \rangle$ at $\omega = 1$ and $\omega = 10$ almost coincide (similar for $\langle \hat{F}_\omega(n, N) \rangle$). For the ergodic case ($T_c = 10$), this is a visual artifact because the mixing estimator at $\omega = 10$ decreases much faster than that at $\omega = 1$. In turn, the weak dependence of the estimator on ω for large ω is expected for nonergodic CTRW due to the nontrivial limiting relation Eqs. (13) and (14).

The standard deviation of the mixing estimator is close to that given by square root of Eq. (11) for Brownian motion for $T_c = 10$, while it is larger for the nonergodic cases $T_c = 10^2$ and $T_c = 10^3$ (similar for the ergodicity estimator). As for the mean value, the standard deviation does not much depend on ω (once ω is large enough). The minimum of the standard deviation at an intermediate n for the nonergodic cases can be related to vanishing of the mean value when it crosses the horizontal axis.

4. Geometric Brownian motion

We consider geometric (or exponential) Brownian motion $X(t)$, which is the basic model in finance, in particular, in the Black-Scholes model for option pricing [36]. This stochastic

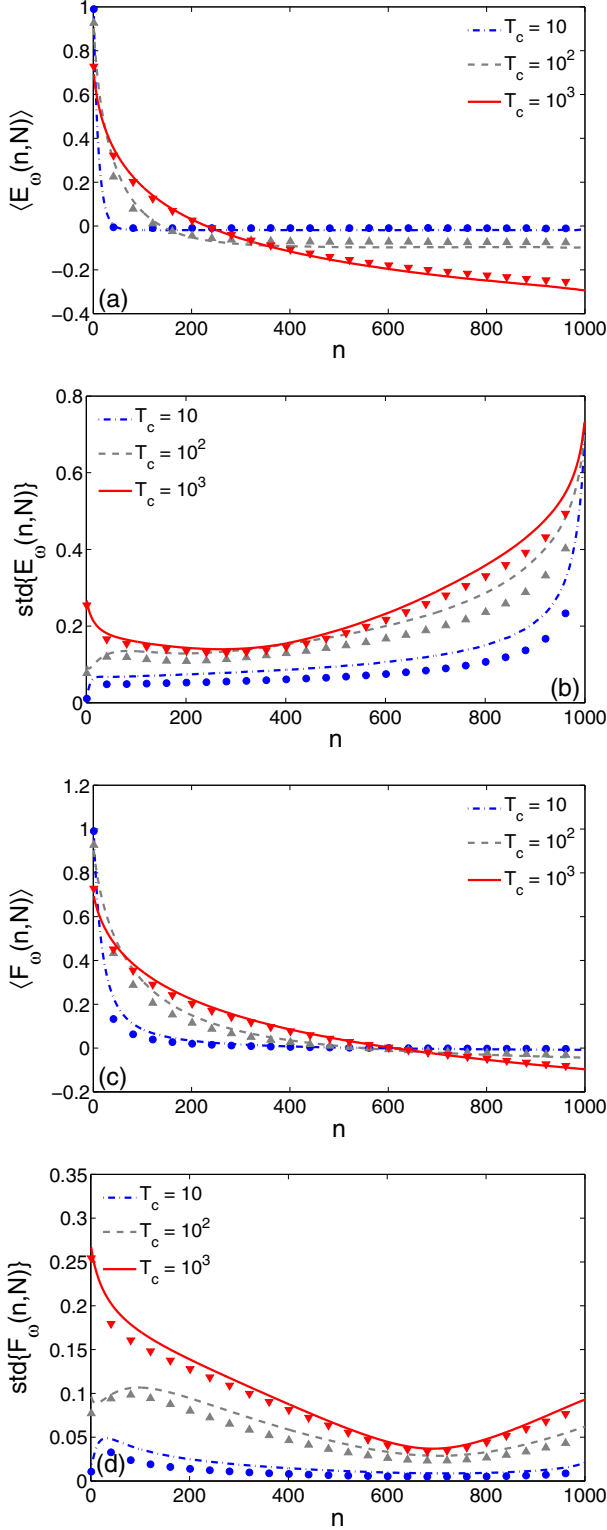


FIG. 15. The mean (a, c) and standard deviation (b, d) of the mixing (a, b) and ergodicity (c, d) estimators at $\omega = 1$ (lines) and $\omega = 10$ (symbols) for CTRW with $N = 1000$, $\alpha = 0.7$, $\sigma = 1$, $\delta_s = 1$, and exponential cutoff at $T_c = 10, 10^2, 10^3$.

process can be expressed as

$$X(t) = X(0) \exp[(\mu - \sigma^2/2)t + \sigma W(t)], \quad (\text{D8})$$

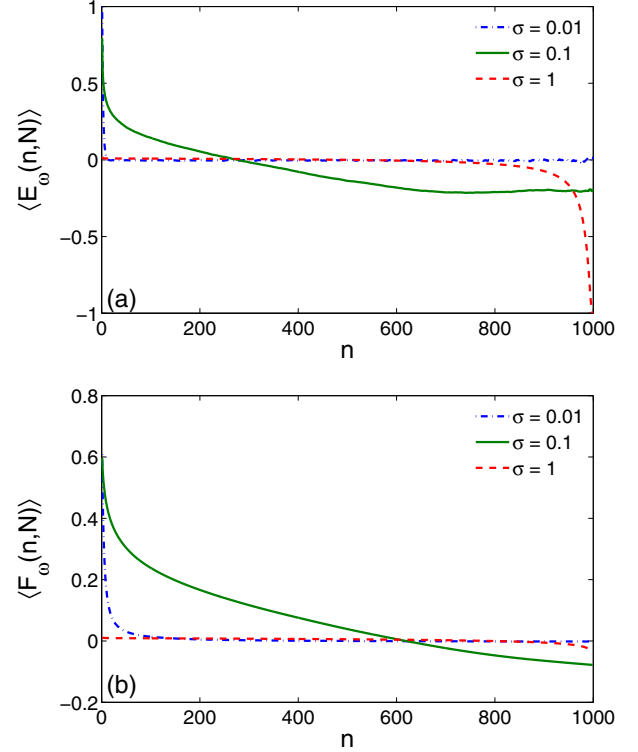


FIG. 16. The mean mixing (a) and ergodicity (b) estimators at $\omega = 1$ as a function of n for geometric Brownian motion with $\mu = 0$ and $\sigma = 0.01, \sigma = 0.1$, and $\sigma = 1$. Each generated trajectory was renormalized by the empirical standard deviation of its increments in order to get comparable results for different σ . The mean was computed numerically by averaging over 1000 trajectories.

where μ and σ are drift and standard deviation, $W(t)$ is a Wiener process (a standard Brownian motion), and the term $(\mu - \sigma^2/2)t$ is explicitly added in order to prevent exponential growth of the variance of $X(t)$. This nonstationary process was recently reported to be nonergodic [26] that may eventually affect current views on trading strategies [32]. After a random exploration time, the trajectory of geometric Brownian motion tends to remain close to 0 for a very long time, which explains the nonergodic behavior.

Figure 16 shows the mean mixing and ergodicity estimators at $\omega = 1$ as a function of n for geometric Brownian motion with $\mu = 0$. During the simulation time ($N = 1000$), the gBm with $\sigma = 0.01$ does not have enough time to be stuck near 0, yielding a rapid decay of both estimators (dash-dotted line). This is a finite-length effect: much longer trajectories would attend the “trapped” state near 0 and thus exhibit nonergodic behavior (not shown). Instead of increasing the trajectory length, we take larger σ for which the trapped state is reached earlier on average. The nonmixing and nonergodic behavior is clearly seen for $\sigma = 0.1$ and $\sigma = 1$. The latter case is also instructive to illustrate that the estimator can take very small values for moderate n for a nonergodic process. This is due to the fact that a large part of the trajectory is almost 0. Inspecting the whole dependence on n can thus be informative.

APPENDIX E: MATLAB CODE

For completeness, we provide a short Matlab code that can be directly applied for analyzing single-particle tracking data.

```
function [E,F] = EFestimator(X,omega);
% This Matlab function implements the improved mixing and ergodicity estimators
% by Y. Lanoiselee and D. Grebenkov
% INPUT: X - vector containing positions of the analyzed trajectory
%         omega - (optional) frequency (the default value is 2)
% OUTPUT: E - the real part of the mixing estimator as a function of n
%         F - the real part of the ergodicity estimator as a function of n
if (nargin < 2) omega = 2; end % Default value for omega
N = length(X)-1; % Trajectory points are enumerated as X(0), ..., X(N)
X = X/std(diff(X)); % Normalization by the empirical standard deviation of displacements
for n=0:N,
    D(n+1) = sum( exp( (1i)*omega*(X(n+1:end) - X(1:end-n)) ) )/(N-n+1);
end
E = D - abs(sum( exp((1i)*omega*X) ))^2/N/(N+1) + 1/N;
for n=1:N, F(n) = sum( E(2:n+1) )/n; end
F(N+1) = NaN; % The last point is not defined
end % end of the function
```

-
- [1] A. V. Weigel, B. Simon, M. M. Tamkun, and D. Krapf, Ergodic and nonergodic processes coexist in the plasma membrane as observed by single-molecule tracking, *Proc. Natl. Acad. Sci. USA* **108**, 6438 (2011).
- [2] J.-H. Jeon, V. Tejedor, S. Burov, E. Barkai, C. Selhuber-Unkel, K. Berg-Sorensen, L. Oddershede, and R. Metzler, In Vivo Anomalous Diffusion and Weak Ergodicity Breaking of Lipid Granules, *Phys. Rev. Lett.* **106**, 048103 (2011).
- [3] E. Barkai, Y. Garini, and R. Metzler, Strange kinetics of single molecules in living cells, *Phys. Today* **65**, 29 (2012).
- [4] I. Y. Wong, M. L. Gardel, D. R. Reichman, E. R. Weeks, M. T. Valentine, A. R. Bausch, and D. A. Weitz, Anomalous Diffusion Probes Microstructure Dynamics of Entangled F-Actin Networks, *Phys. Rev. Lett.* **92**, 178101 (2004).
- [5] X. Brokmann, J.-P. Hermier, G. Messin, P. Desbailles, J.-P. Bouchaud, and M. Dahan, Statistical Aging and Nonergodicity in the Fluorescence of Single Nanocrystals, *Phys. Rev. Lett.* **90**, 120601 (2003).
- [6] G. Margolin and E. Barkai, Nonergodicity of Blinking Nanocrystals and Other Levy-Walk Processes, *Phys. Rev. Lett.* **94**, 080601 (2005).
- [7] G. Margolin and E. Barkai, Nonergodicity of a time series obeying Levy statistics, *J. Stat. Phys.* **122**, 137 (2006).
- [8] S. Burov, J.-H. Jeon, R. Metzler, and E. Barkai, Single particle tracking in systems showing anomalous diffusion: The role of weak ergodicity breaking, *Phys. Chem. Chem. Phys.* **13**, 1800 (2011).
- [9] R. Metzler, J.-H. Jeon, A. Cherstvy, and E. Barkai, Anomalous diffusion models and their properties: Non-stationarity, non-ergodicity, and ageing at the centenary of single particle tracking, *Phys. Chem. Chem. Phys.* **16**, 24128 (2014).
- [10] M. Magdziarz and A. Weron, Ergodic properties of anomalous diffusion processes, *Ann. Phys.* **326**, 2431 (2011).
- [11] A. I. Khinchin, *Mathematical Foundations of Statistical Mechanics* (Dover, New York, 1949).
- [12] L. C. Lapas, R. Morgado, M. H. Vainstein, J. M. Rubi, and F. A. Oliveira, Khinchin Theorem and Anomalous Diffusion, *Phys. Rev. Lett.* **101**, 230602 (2008).
- [13] S. Burov, R. Metzler, and E. Barkai, Aging and nonergodicity beyond the Khinchin theorem, *Proc. Natl. Acad. Sci. USA* **107**, 13228 (2010).
- [14] M. Magdziarz and A. Weron, Anomalous diffusion: Testing ergodicity breaking in experimental data, *Phys. Rev. E* **84**, 051138 (2011).
- [15] J. Janczura and A. Weron, Ergodicity testing for anomalous diffusion: Small sample statistics, *J. Chem. Phys.* **142**, 144103 (2015).
- [16] J. A. Dix and A. S. Verkman, Crowding Effects on Diffusion in Solutions and Cells, *Annu. Rev. Biophys.* **37**, 247 (2008).
- [17] I. M. Sokolov, Models of anomalous diffusion in crowded environments, *Soft Matter* **8**, 9043 (2012).
- [18] F. Höfling and T. Franosch, Anomalous transport in the crowded world of biological cells, *Rep. Progr. Phys.* **76**, 046602 (2013).
- [19] A. N. Kolmogorov, Wiener'sche Spiralen und einige andere interessante Kurven im Hilbertschen Raum, *C. R. (Doklady) Acad. Sci. URSS (N. S.)* **26**, 115 (1940).
- [20] B. Mandelbrot and J. W. van Ness, Fractional Brownian motions, fractional noises and applications, *SIAM Rev.* **10**, 422 (1968).
- [21] Y. Gefen, A. Aharony, and S. Alexander, Anomalous Diffusion on Percolating Clusters, *Phys. Rev. Lett.* **50**, 77 (1983).
- [22] J.-P. Bouchaud and A. Georges, Anomalous diffusion in disordered media: Statistical mechanisms, models and physical applications, *Phys. Rep.* **195**, 127 (1990).
- [23] J. Klafter and I. M. Sokolov, *First Steps in Random Walks: From Tools to Applications* (Oxford University Press, Oxford, 2011).

- [24] F. Thiel and I. M. Sokolov, Scaled Brownian motion as a mean-field model for continuous-time random walks, *Phys. Rev. E* **89**, 012115 (2014).
- [25] J.-H. Jeon, A. V. Chechkin, and R. Metzler, Scaled Brownian motion: A paradoxical process with a time dependent diffusivity for the description of anomalous diffusion, *Phys. Chem. Chem. Phys.* **16**, 15811 (2014).
- [26] O. Peters and W. Klein, Ergodicity Breaking in Geometric Brownian Motion, *Phys. Rev. Lett.* **110**, 100603 (2013).
- [27] G. Bel and E. Barkai, Weak Ergodicity Breaking in the Continuous-Time Random Walk, *Phys. Rev. Lett.* **94**, 240602 (2005).
- [28] A. J. Berglund, Statistics of camera-based single-particle tracking, *Phys. Rev. E* **82**, 011917 (2010).
- [29] M. P. Backlund, R. Joyner, and W. E. Moerner, Chromosomal locus tracking with proper accounting of static and dynamic errors, *Phys. Rev. E* **91**, 062716 (2015).
- [30] A. Lubelski, I. M. Sokolov, and J. Klafter, Nonergodicity Mimics Inhomogeneity in Single Particle Tracking, *Phys. Rev. Lett.* **100**, 250602 (2008).
- [31] P. Massignan, C. Manzo, J. A. Torreno-Pina, M. F. Garcia-Parajo, M. Lewenstein, and G. J. Lapeyre, Nonergodic Subdiffusion from Brownian Motion in an Inhomogeneous Medium, *Phys. Rev. Lett.* **112**, 150603 (2014).
- [32] O. Peters, Optimal leverage from non-ergodicity, *Quant. Finance* **11**, 1593 (2011).
- [33] I. Golding and E. C. Cox, Physical Nature of Bacterial Cytoplasm, *Phys. Rev. Lett.* **96**, 098102 (2006).
- [34] E. Bertseva, D. S. Grebenkov, P. Schmidhauser, S. Gribkova, S. Jeney, and L. Forró, Optical trapping microrheology in cultured human cells, *Eur. Phys. J. E* **35**, 63 (2012).
- [35] D. S. Grebenkov, M. Vahabi, E. Bertseva, L. Forro, and S. Jeney, Hydrodynamic and subdiffusive motion of tracers in a viscoelastic medium, *Phys. Rev. E* **88**, 040701(R) (2013).
- [36] J. C. Hull, *Options, Futures and Other Derivatives*, 7th ed. (Pearson Prentice Hall, Upper Saddle River, NJ, 2009).
- [37] M. J. Saxton and K. Jacobson, Single-particle tracking: Applications to membrane dynamics, *Annu. Rev. Biophys. Biomol. Struct.* **26**, 373 (1997).
- [38] D. Arcizet, B. Meier, E. Sackmann, J. O. Rädler, and D. Heinrich, Temporal Analysis of Active and Passive Transport in Living Cells, *Phys. Rev. Lett.* **101**, 248103 (2008).
- [39] M. H. G. Duits, Y. Li, S. A. Vanapalli, and F. Mugele, Mapping of spatiotemporal heterogeneous particle dynamics in living cells, *Phys. Rev. E* **79**, 051910 (2009).
- [40] M. Magdziarz, A. Weron, K. Burnecki, and J. Klafter, Fractional Brownian Motion Versus the Continuous-Time Random Walk: A Simple Test for Subdiffusive Dynamics, *Phys. Rev. Lett.* **103**, 180602 (2009).
- [41] Y. Meroz, I. M. Sokolov, and J. Klafter, Subdiffusion of mixed origins: When ergodicity and nonergodicity coexist, *Phys. Rev. E* **81**, 010101(R) (2010).
- [42] V. Tejedor, O. Bénichou, R. Voituriez, R. Jungmann, F. Simmel, C. Selhuber-Unkel, L. B. Oddershede, and R. Metzler, Quantitative analysis of single particle trajectories: Mean maximal excursion method, *Biophys. J.* **98**, 1364 (2010).
- [43] E. Kepten, I. Bronshtein, and Y. Garini, Ergodicity convergence test suggests telomere motion obeys fractional dynamics, *Phys. Rev. E* **83**, 041919 (2011).
- [44] S. Türkcan, A. Alexandrou, and J.-B. Masson, A Bayesian inference scheme to extract diffusivity and potential fields from confined single-molecule trajectories, *Biophys. J.* **102**, 2288 (2012).
- [45] Y. Meroz, I. M. Sokolov, and J. Klafter, Test for Determining a Subdiffusive Model in Ergodic Systems from Single Trajectories, *Phys. Rev. Lett.* **110**, 090601 (2013).
- [46] M. Weiss, Single-particle tracking data reveal anticorrelated fractional Brownian motion in crowded fluids, *Phys. Rev. E* **88**, 010101(R) (2013).
- [47] E. Kepten, I. Bronshtein, and Y. Garini, Improved estimation of anomalous diffusion exponents in single-particle tracking experiments, *Phys. Rev. E* **87**, 052713 (2013).
- [48] C. L. Vestergaard, P. C. Blainey, and H. Flyvbjerg, Optimal estimation of diffusion coefficients from single-particle trajectories, *Phys. Rev. E* **89**, 022726 (2014).
- [49] I. S. Gradshteyn and I. M. Ryzhik, *Table of Integrals, Series, and Products* (Academic Press, San Diego, 1980).
- [50] D. Stauffer and A. Aharony, *Introduction to Percolation Theory*, 2nd ed. (Taylor & Francis, London, 2003).
- [51] B. Nienhuis, Critical behavior of two-dimensional spin models and charge asymmetry in the coulomb gas, *J. Stat. Phys.* **34**, 731 (1984).
- [52] G. Bottazzi, *On the Pareto Type III Distribution*, LEM Working Paper Series 2007/07 (2007).
- [53] G. Samorodnitsky and M. S. Taqqu, *Stable Non-Gaussian Random Processes: Stochastic Models with Infinite Variance* (Chapman and Hall, New York, 1994).
- [54] Historically, first papers on mixing and ergodic properties of SID processes required a dynamical functional in a form similar to Eq. (1) to vanish as $n \rightarrow \infty$ for any frequency ω (for details, see Ref. [53], chap. 14.4). In other words, to validate the mixing property, one needed to check the behavior of the functional for any ω that was impractical. Magdziarz and Weron have made a significant improvement by reducing the analysis to a single value of ω (they set $\omega = 1$). Here, we reintroduce the frequency ω as a means to renormalize the process, but we still consider a single value of ω (which may differ from 1).
- [55] Note that Magdziarz and Weron have analyzed the same set of experimental trajectories of mRNA molecules reported in Ref. [33]. As a consequence, Fig. 9(a) resembles Fig. 6(a) from Ref. [14], except for the opposite sign which may be related to different normalizations of the increments and the shifted summation range ($k = 1, \dots, n$ instead of $k = 0, \dots, n - 1$) in the ergodicity estimator that was actually used in Ref. [14] (private communication by M. Magdziarz).